Chemical Reactivity

Volume 1: Theories and Principles

Edited by

Savaş Kaya

László von Szentpály

Goncagül Serdaroğlu

Lei Guo

ELSEVIER

Elsevier
Radarweg 29, PO Box 211, 1000 AE Amsterdam, Netherlands
The Boulevard, Langford Lane, Kidlington, Oxford OX5 1GB, United Kingdom
50 Hampshire Street, 5th Floor, Cambridge, MA 02139, United States

Notices

Knowledge and best practice in this field are constantly changing. As new research and experience broaden our understanding, changes in research methods, professional practices, or medical treatment may become necessary.

Practitioners and researchers must always rely on their own experience and knowledge in evaluating and using any information, methods, compounds, or experiments described herein. In using such information or methods they should be mindful of their own safety and the safety of others, including parties for whom they have a professional responsibility.

To the fullest extent of the law, neither the Publisher nor the authors, contributors, or editors, assume any liability for any injury and/or damage to persons or property as a matter of products liability, negligence or otherwise, or from any use or operation of any methods, products, instructions, or ideas contained in the material herein.

ISBN: 978-0-323-90257-1

Publisher: Candice Janco
Acquisitions Editor: Charles Bath
Editorial Project Manager: Catherine Costello
Production Project Manager: Sruthi Satheesh
Cover Designer: Christian Bilbow

Typeset by VTeX

Contents

12. Main concepts and applications of DFTB approach

Elyor Berdimurodov, Lei Guo, Abduvali Kholikov, Khamdam Akbarov, and Savaş Kaya

13. Chemical reactivity insights from the use of constrained methods

Andrés Cedillo

14. On the analysis of the Fukui function

P. Fuentealba and C. Cárdenas

Contributors

Khamdam Akbarov, Faculty of Chemistry, National University of Uzbekistan, Tashkent, Uzbekistan

P.D. Astudillo-Sánchez, Basic and Applied Sciences Department, University of Guadalajara, Tonalá, Jal., Mexico

Leandro Ayarde-Henríquez, Universidad Andres Bello, Departamento de Ciencias Químicas, Centro de Química Teórica y Computacional (CQT&C), Facultad de Ciencias Exactas, Santiago, Chile
School of Physics, Trinity College Dublin, Dublin, Ireland

Elyor Berdimurodov, Faculty of Chemistry, National University of Uzbekistan, Tashkent, Uzbekistan

Uğur Bozkaya, Department of Chemistry, Hacettepe University, Ankara, Turkey

Ramon Carbó-Dorca, Institut de Química Computacional i Catàlisi, Universitat de Girona, Girona, Catalonia, Spain

C. Cárdenas, Departamento de Física, Facultad de Ciencias, Universidad de Chile, Santiago, Chile
Centro para el Desarrollo de la Nanociencia y la Nanotecnología (CEDENNA), Santiago, Chile

Andrés Cedillo, Departamento de Química, Universidad Autónoma Metropolitana-Iztapalapa, México, CDMX, México

Tanmoy Chakraborty, Department of Chemistry and Biochemistry, Sharda School of Basic Sciences and Research, Sharda University, Greater Noida, Uttar Pradesh, India

Eduardo Chamorro, Universidad Andres Bello, Departamento de Ciencias Químicas, Centro de Química Teórica y Computacional (CQT&C), Facultad de Ciencias Exactas, Santiago, Chile

Héctor Hernández Corzo, National Center for Computational Sciences, Oak Ridge Leadership Computing Facility, Oak Ridge National laboratory, Oak Ridge, TN, United States

Manuel Díaz-Tinoco, Department of Chemistry and Biochemistry, Auburn University, Auburn, AL, United States

Mario Duque-Noreña, Universidad Andres Bello, Departamento de Ciencias Químicas, Centro de Química Teórica y Computacional (CQT&C), Facultad de Ciencias Exactas, Santiago, Chile

Rocío Durán, Centro de Bioinformática, Simulación y Modelado (CBSM), Facultad de Ingeniería, and Instituto de Investigación Interdisciplinaria (I^3), Vicerrectoría Académica, Universidad de Talca, Talca, Chile

R. Flores-Moreno, Chemistry Department, University of Guadalajara, Guadalajara, Jal., Mexico

J.A. Flores-Ramos, Chemistry Department, University of Guadalajara, Guadalajara, Jal., Mexico

Evelio Francisco, Department of Physical and Analytical Chemistry, Faculty of Chemistry, University of Oviedo, Oviedo, Spain

Marek Freindorf, CATCO Group, Chemistry Department, Southern Methodist University, Dallas, TX, United States

P. Fuentealba, Departamento de Física, Facultad de Ciencias, Universidad de Chile, Santiago, Chile
Centro para el Desarrollo de la Nanociencia y la Nanotecnología (CEDENNA), Santiago, Chile

Miguel Gallegos, Department of Physical and Analytical Chemistry, Faculty of Chemistry, University of Oviedo, Oviedo, Spain

Cristian Guerra, Universidad Andres Bello, Departamento de Ciencias Químicas, Centro de Química Teórica y Computacional (CQT&C), Facultad de Ciencias Exactas, Santiago, Chile

Lei Guo, School of Materials and Chemical Engineering, Tongren University, Tongren, China

Savaş Kaya, Cumhuriyet University, Faculty of Science, Department of Chemistry, Sivas, Turkey

Abduvali Kholikov, Faculty of Chemistry, National University of Uzbekistan, Tashkent, Uzbekistan

Ludwik Komorowski, Department of Physical and Quantum Chemistry, Wrocław University of Science and Technology, Wrocław, Poland

Elfi Kraka, CATCO Group, Chemistry Department, Southern Methodist University, Dallas, TX, United States

Ricardo A. Matute, Centro Integrativo de Biología y Química Aplicada (CIBQA), Universidad Bernardo O'Higgins, Santiago, Chile
Division of Chemistry and Chemical Engineering, California Institute of Technology, Pasadena, CA, United States

Á. Nagy, Department of Theoretical Physics, University of Debrecen, Debrecen, Hungary

Roman F. Nalewajski, Department of Theoretical Chemistry, Jagiellonian University, Cracow, Poland

Piotr Ordon, Department of Physics and Biophysics, Wrocław University of Environmental and Life Sciences, Wrocław, Poland

Daniela E. Ortega, Centro Integrativo de Biología y Química Aplicada (CIBQA), Universidad Bernardo O'Higgins, Santiago, Chile

J.V. Ortiz, Department of Chemistry and Biochemistry, Auburn University, Auburn, AL, United States

Filip Pawłowski, Department of Chemistry and Biochemistry, Auburn University, Auburn, AL, United States

Ángel Martín Pendás, Department of Physical and Analytical Chemistry, Faculty of Chemistry, University of Oviedo, Oviedo, Spain

Patricia Pérez, Universidad Andres Bello, Departamento de Ciencias Químicas, Centro de Química Teórica y Computacional (CQT&C), Facultad de Ciencias Exactas, Santiago, Chile

Martin Rahm, Department of Chemistry and Chemical Engineering, Chalmers University of Technology, Gothenburg, Sweden

Elizabeth Rincón, Facultad de Ciencias, Instituto de Ciencias Químicas, Valdivia, Chile

J. Valdez-Ruvalcaba, Chemistry Department, University of Guadalajara, Guadalajara, Jal., Mexico

Nery Villegas-Escobar, Departamento de Físico-Química, Facultad de Ciencias Químicas, Universidad de Concepción, Concepción, Chile

László von Szentpály, Institute for Theoretical Chemistry, University of Stuttgart, Stuttgart, Germany

Emily Z. Wang, Department of Molecular Medicine, Cornell College of Veterinary Medicine, Cornell University, Ithaca, NY, United States

Yi-Gui Wang, Department of Chemistry, Southern Connecticut State University, New Haven, CT, United States

Chapter 9

Reaction fragility method: monitoring evolution of atoms and bonds on a reaction path

Piotr Ordon[a] **and Ludwik Komorowski**[b]

[a]*Department of Physics and Biophysics, Wrocław University of Environmental and Life Sciences, Wrocław, Poland,* [b]*Department of Physical and Quantum Chemistry, Wrocław University of Science and Technology, Wrocław, Poland*

9.1 Introduction: the search for atoms

The formal structure of the Conceptual Density Functional Theory (CDFT) has expanded over the years to the well-organized, quasithermodynamic system concentrated on exploration of the energy functional $E[\rho(\mathbf{r})]$ in quantification of properties of molecules. The global quantities characterizing atomic and molecular entities are [1–4]: chemical potential $\mu = [\partial E/\partial N]_v$, hardness $\eta = \left[\partial^2 E/\partial N^2\right]_v$, and softness $S = 1/\eta$. The local quantities describe a response of the density function to the change in N or μ, namely Fukui function $f(\mathbf{r}) = [\partial\rho(\mathbf{r})/\partial N]_v$ and local softness $s(\mathbf{r}) = [\partial\rho(\mathbf{r})/\partial\mu]_v$. Contracting these local quantities to atoms bonded in molecules has long been recognized as an important challenge on the way to CDFT applications in practical chemistry. However, the results have been limited to various types of approximations [5–12], far from expectations of chemistry where the reality of bonded atoms has been a cornerstone for consideration of reactivity. The difficulty has long been recognized: neither the QTAIM method [13] nor the Hirschfeld partition had produced more than a '*noumenon*' – "*an object of purely intellectual intuition* (. . .) *subject to arbitrary* (*but disciplined*) *personal choice when specificity is desired*" [14].

For practical reasons, the closed-system representation (canonical ensemble) has been dominating in the analyses, $E[N; v(\mathbf{r})]$. The linear response function (LRF), combining the electron density $\rho(\mathbf{r})$ and the external potential $v(\mathbf{r})$ in a closed system containing N electrons, has been most naturally introduced as a functional derivative playing the key role in the chemistry oriented analyses [1]: $\omega(\mathbf{r}, \mathbf{r}') = \left[\delta\rho(\mathbf{r})/\delta v\left(\mathbf{r}'\right)\right]_N$. The properties of this kernel function have been subject of many studies concentrated on bonded atoms by observation of the polarization of the electron density $\rho(\mathbf{r})$ in a system upon disturbing the local

Chemical Reactivity. https://doi.org/10.1016/B978-0-32-390257-1.00016-4

external potential $\delta v\left(\mathbf{r}'\right)$. Geerlings et al. have demonstrated how the fundamental notion of LRF has been tentatively explored in analysis of local properties of atoms-in-molecules [15]. Boisdenghien et al. have presented an electron energy expansion in the Taylor series; attractive two- and one-dimensional projections of the LRF as $\omega(\mathbf{r}, 0)$ for atoms have resulted [16,17].

Another approach to LRF by the above authors was aimed *via* polarizability of atoms and molecules that has been reasonably reproduced by using computable results for $\omega(\mathbf{r}, \mathbf{r}')$ [18]. The formal link between the LRF and the polarizability tensor has been first proposed by Vela and Gazques [19]. It was dwelled upon by other authors [20,21] and the polarization-justified Fukui indices have been developed on this ground by Komorowski et al. [22]. The LRF condensed to atoms has been proposed by Sablon et al. by an arbitrary integration of the $\omega(\mathbf{r}, \mathbf{r}')$ kernel; the result has been explored to quantify inductive and resonance effects [23].

The new perspective for discerning atoms in the CDFT formalism has been opened by exploration of the Hellmann–Feynman (H–F) forces on the nuclei. In the absence of external fields other then from atomic nuclei, the disturbance in the external potential $\Delta v(\mathbf{r})$ is uniquely defined by shifts of the nuclei in a system $\{\Delta \mathbf{R}_i\}$. Consequently, alternative representations for the closed and open systems have been introduced $E[N; \{\mathbf{R}\}]$ and $E[\mu; \{\mathbf{R}\}]$ [24–27]. Energy derivatives over displacement of nuclei $\Delta \mathbf{R}_i$ in these representations have fundamental physical meaning of force, force constant, and anharmonicities associated with displacement of atomic nuclei. They all directly describe properties of atoms bound within the system and characterize atomic contacts. Since forces are entirely determined by the electron density function, there is no need to artificially condense any local quantities for determining properties of individual atoms.

The original concept of the Hellmann–Feynman force uniquely identifies atomic nuclei in molecules [28,29], $\mathbf{F}_A = -\nabla_A E = \mathbf{F}_A^{el} + \mathbf{F}_A^{nn}$. Early consideration of the origin of forces and consequences thereof have been provided by Nakatsuji [30,31]. The link between the H–F forces and the CDFT formalism has been first shown by Cohen et al. [32], the authors also introduced the new derivative of chemical potential under the name nuclear reactivity, $\mathbf{\Phi}_A = (\partial \mathbf{F}_A / \partial N)_{\{\mathbf{R}\}} = -\nabla_A \mu$. The concept has been explored by other authors, however, initial hopes for directly indexing reactivity of bonded atoms by $\mathbf{\Phi}_A$ were in vain [26,33,34]. In the latest work by Laplaza et al., the coupling between the orbital energies and the shifts of the nuclei has been analyzed [35].

The nuclear stiffness has been introduced as the next corresponding derivative of global hardness by Ordon et al. as an extension of this idea, namely $\mathbf{G}_A = \left(\partial^2 \mathbf{F}_A / \partial N^2\right)_{\{\mathbf{R}\}} = \nabla_A \eta$ [25]. The whole body of energy derivatives in the representation of atomic coordinates both in the closed ($N = const.$) and open ($\mu = const.$) systems has been formulated; their renormalization has also been demonstrated [36,37]. The vital result of that effort focused directly on atoms identified by the H–F forces was the discovery of vibrational softening of

molecules by the authors of this work [38–40] with perspectives for applications to explosive reactions [41]. The linear response function has been essential for bridging the energy derivatives in the basic CDFT formalism and their counterparts built on $E[N;\{\mathbf{R}\}]$ function [42].

A significant contribution to the theory on the role of atoms in chemical reactivity has been elaborated by Nalewajski [43,44] with the goal to: "*understand the subtle interplay between the geometrical and/or electronic degrees of freedom of both isolated molecules and the reactive systems*" [45]. The coupling has been described in the atomic discretization at the CSA level, originally proposed by Nalewajski [43]. This sophisticated approach has been founded on the electron preceding perspective ("chemical thinking") and had by necessity combined the basic parameters from two nonequivalent sources: the exact positions of nuclei and exact forces thereon have been used in parallel to the populations of the point-atoms, reasonably calculated (albeit arbitrarily defined) from the equalization of the chemical potential in the system. The lasting value of this analysis was in formulating the geometrical minimum energy coordinate (MEC) concept for tracing the changes in electronic structure of a reacting system.

9.2 Exposing the electron energy by the force constants analysis

Recently we have exposed the fresh practical power of the application of the vector analysis to the derivatives of the H–F force along a defined reaction path (IRC), meeting the MEC condition. We have found that the divergence of H–F force contains solely the electronic energy of a system, since nuclear–nuclear contributions vanish by the Laplace law [46]. This valuable property has been first mentioned by King et al. as the frequency sum rule [47–49]. The authors attempted to characterize bond properties with the use force divergences calling them effective force constants and noticed that the electronic energy contributes exclusively to the divergence of the H–F force. Decius and Wilson also used that sum rule, however, their work has been limited to the isotopic effects [50]. The even earlier deep analysis by Salem contained the clear formulation for the derivatives of the H–F forces [51].

We have established that the H–F force divergences calculated along the reaction path, represent a potential source of quantitative information on evolution of the electron density within a reacting system [52]. This is definitely an approach from the atomic and bonding perspective. The H–F force divergences for any system of n atoms form the novel DF Connectivity Matrix $\underline{\underline{\mathbf{C}}}$ that describes electronic properties of the system in the long desired atomic resolution. This DF Connectivity Matrix has a different meaning than the old, arbitrary concept of the Atomic Connectivity Matrix (ACM) first proposed by Spialter [53,54] and developed by his followers within the graph theory [55–59]; the idea has been applied even to an analysis of crystal structures [60], with appropriate modifications as to reflect the bond valences [61].

Our DF Connectivity Matrix delivers theoretical description of the atomic valences and bond orders providing readily available and exact numerical data [62]. We obtain the elements of the DF Connectivity Matrix elements (C_{AA}, C_{AB} – cumulative force constants) in the harmonic approximation by appropriate summation of the elements of the Cartesian Hessian. The harmonic oscillator's regime seems to be limiting; however, when C_{AA} and C_{AB} are calculated for a sequence of stationary states along the IRC, their step-by-step variations unveil the process beyond the harmonic condition: modification of atomic bonds (and valences) as a result of the ongoing chemical reaction. This straightforward method to picture the mechanism of the chemical reaction leads to the analogous results [63] as observations of the reaction path curvatures provided with the advanced normal modes considerations by Kraka et al. (adiabatic internal vibrational mode AIMO [64]), within their unified reaction valley approach (URVA) [65–71].

Recently we have investigated in depth the derivatives of the elements of the DF connectivity matrix over reaction progress ($dC_{\mathrm{AA}}/d\xi$, $dC_{\mathrm{AB}}/d\xi$). The working term Reaction Fragility (RF) has been adopted for those derivatives [52]. They were found to reproduce very accurately the evolution of common atomic properties along a reaction path: the evolution of the atomic valence and the bond orders, respectively [63,72]. The atomic fragilities also provide proper measure for the contribution of an atom to the global reaction force [73] $F_{\xi} = dE/d\xi$.

Since the H–F forces themselves, as well as their divergences, are readily available in standard quantum chemical computations, the method can be routinely applied for monitoring and imaging changes in reacting systems, traced along a reaction path. For this task we have applied the IRC formalism [74–76]. The spectrum-like diagrams of changes along a reaction have also been demonstrated for the potential energy of bonded atoms, naturally apportioned as fractions of the potential energy of a system [77]. The method provides description of atoms and their bonds with no need for the common arbitrary definitions assigning atomic volumes or populations [78,79].

We devote this present article to revealing links between the reaction fragility formalism based on the DF Connectivity Matrix, and the theoretical framework of conceptual DFT where the density linear response function plays central role. Novel properties of the electron density function that can be deduced form the DF Connectivity Matrix formalism have been presented first (Section 9.3). The link between the CDFT derivatives and their counterparts in the reaction fragility analysis is outlined. The energy expansion has been presented in the representation $E[N; \{\mathbf{R}\}]$; it is followed by an interpretation of the role of DF Connectivity Matrix in tracing the vibrational energy attributed to individual atoms. The atomic fragility modes, an alternative to the normal mode analysis, have finally been presented (Section 9.4). Application to a chemical reaction within the IRC formalism follows in Section 9.5. The numerical analysis of the proton migration in formamide molecule has been presented for the sake of

illustration the power of the atomic fragility modes in monitoring the role of atoms in a reaction (Section 9.6).

9.3 The electron density gradient in the DF connectivity matrix formalism

Recently we have derived direct relations between the force divergences essential for the Reaction Fragility concept and the electron density gradient [77]. We consider here a molecule as the system of atoms in an electronically stationary state, with no external field, other than generated by the nuclei in the system. The divergences of H–F forces in a molecule built with n atoms form the $n \times n$ DF connectivity matrix. As we have recently demonstrated, the elements of the connectivity matrix are exactly [77,80]:

$$C_{AA} = \nabla_A \cdot \mathbf{F}_A = \int \boldsymbol{\varepsilon}_A(\mathbf{r}) \cdot [\nabla\rho(\mathbf{r}) + \nabla_A\rho(\mathbf{r})]\, d\mathbf{r}, \tag{9.1}$$

$$C_{B\neq A} = \nabla_{B\neq A} \cdot \mathbf{F}_A = \int \boldsymbol{\varepsilon}_A(\mathbf{r}) \cdot \left[\nabla_{B\neq A}\rho(\mathbf{r})\right] d\mathbf{r}. \tag{9.2}$$

For the specific notation and derivations, see the Appendix 9.A.1 and 9.A.2, respectively. The sum rule has also been established, $\sum_B C_{BA} = \sum_A C_{BA} = 0$, hence $C_{AA} = -\sum_{B\neq A} C_{BA}$ [46].

9.3.1 From the DF connectivity matrix to the electron density gradient

By combining the above sum rule with Eqs. (9.1) and (9.2), a novel condition for the stationary electron density has been noticed, namely

$$\int \boldsymbol{\varepsilon}_A(\mathbf{r}) \cdot \left[\nabla\rho(\mathbf{r}) + \sum_B \nabla_B\rho(\mathbf{r})\right] d\mathbf{r} = 0. \tag{9.3}$$

This condition is general and no symmetry restrictions have been invoked. Since the solution for $\rho(\mathbf{r})$ in Eq. (9.3) must be unique [81], and Eq. (9.3) holds separately for every atom (A) in a system, the natural property of the electron density in an external field from all nuclei emerges is

$$\nabla\rho(\mathbf{r}) = -\sum_B \nabla_B\rho(\mathbf{r}). \tag{9.4}$$

Eq. (9.4) represents potentially important property of the electron density in a system of atoms. For a single atom, it is reduced to the sound identity, $\nabla\rho(\mathbf{r}) = -\nabla_B\rho(\mathbf{r})$. Eq. (9.4) may be transformed into the more specific form, as the density gradient above $\nabla_B\rho(\mathbf{r})$ has only been conceived here as a derivative with no other condition specified. In the closed (canonical) system, it is

conveniently expressed by the electronic response function [46],

$$[\nabla_B \rho(\mathbf{r})]_N = \int \left[\frac{\delta\rho(\mathbf{r})}{\delta v(\mathbf{r}')}\right]_N \frac{dv(\mathbf{r}')}{d\mathbf{R}_B} d\mathbf{r}' = -\int \omega(\mathbf{r},\mathbf{r}')\boldsymbol{\varepsilon}_B(\mathbf{r}')d\mathbf{r}'. \tag{9.5}$$

Hence, Eq. (9.4) leads to a new relation between the density gradient and the linear response function, never exposed hitherto, to the best knowledge of authors, namely

$$\nabla\rho(\mathbf{r}) = \int \omega(\mathbf{r},\mathbf{r}')\boldsymbol{\varepsilon}(\mathbf{r}')d\mathbf{r}'. \tag{9.6}$$

Here $\boldsymbol{\varepsilon}(\mathbf{r}') = \sum_B \boldsymbol{\varepsilon}_B(\mathbf{r}')$ is the electric field from all external sources (nuclei only). This gradient theorem (Eq. (9.6)) provides the novel and much needed interconnection between the electric field and the density gradients, as discussed by Bader on numerous examples [13].

The proof of Eq. (9.6) is straightforward within the CDFT framework, it provides a rationale to the conclusion from Eq. (9.4). By definition, the linear response function in a closed system is $\omega(\mathbf{r},\mathbf{r}') = \left[\delta\rho(\mathbf{r})/\delta v(\mathbf{r}')\right]_N$. Hence,

$$\begin{aligned}\int \omega(\mathbf{r},\mathbf{r}')\boldsymbol{\varepsilon}(\mathbf{r}')d\mathbf{r}' &= \int \left[\frac{\delta\rho(\mathbf{r})}{\delta v(\mathbf{r}')}\right]_N \nabla v(\mathbf{r}')d\mathbf{r}' = \\ &= \int \left[\frac{\delta\rho(\mathbf{r})}{\delta v(\mathbf{r}')}\right]_N \frac{dv(\mathbf{r}')}{d\mathbf{r}'} d\mathbf{r}' = \nabla\rho(\mathbf{r}).\end{aligned} \tag{9.7}$$

9.3.2 Equivalence of the open and closed systems

The density gradient $\nabla\rho(\mathbf{r})$ must not depend on the way it has been calculated. Hence, an alternative for Eq. (9.5) must be checked in the grand-canonical ensemble, appropriate for an open system with the softness kernel $s(\mathbf{r},\mathbf{r}') = -\left[\delta\rho(\mathbf{r})/\delta v(\mathbf{r}')\right]_\mu$, that is,

$$[\nabla_B \rho(\mathbf{r})]_\mu = \int \left[\frac{\delta\rho(\mathbf{r})}{\delta v(\mathbf{r}')}\right]_\mu \frac{dv(\mathbf{r}')}{d\mathbf{R}_B} d\mathbf{r}' = \int s(\mathbf{r},\mathbf{r}')\boldsymbol{\varepsilon}_B(\mathbf{r}')d\mathbf{r}'. \tag{9.8}$$

This is analogous to Eq. (9.5), however, $[\nabla_B\rho(\mathbf{r})]_N$ and $[\nabla_B\rho(\mathbf{r})]_\mu$ are not identical, as can be demonstrated using the well-founded and exact Berkowitz–Parr relation [82], between the response function $\omega(\mathbf{r},\mathbf{r}')$ and the softness kernel $s(\mathbf{r},\mathbf{r}')$,

$$\omega(\mathbf{r},\mathbf{r}') = -s(\mathbf{r},\mathbf{r}') + Sf(\mathbf{r})f(\mathbf{r}'). \tag{9.9}$$

By using this in Eq. (9.5) and applying Eq. (9.8), the difference between gradients calculated in two alternative systems is exposed as

$$[\nabla_B\rho(\mathbf{r})]_N = [\nabla_B\rho(\mathbf{r})]_\mu - s(\mathbf{r})\boldsymbol{\Phi}_B, \tag{9.10}$$

where $s(\mathbf{r}) = \int s(\mathbf{r}, \mathbf{r}')d\mathbf{r}'$ is local softness and $\mathbf{\Phi}_B$ stands for the nuclear reactivity vector. Its connection to the Fukui function is well founded (Eq. (9.11)) [25,26]:

$$\int f(\mathbf{r}')\boldsymbol{\varepsilon}_B(\mathbf{r}')d\mathbf{r}' = \mathbf{\Phi}_B = \left(\frac{\partial \mathbf{F}_B}{\partial N}\right)_{v(r)}, \tag{9.11}$$

Eq. (9.6) for the density gradient $\nabla\rho(\mathbf{r})$ is alternatively formulated in an open system as

$$\nabla\rho(\mathbf{r}) = -\int s(\mathbf{r}, \mathbf{r}')\boldsymbol{\varepsilon}(\mathbf{r}')d\mathbf{r}'. \tag{9.12}$$

By subtracting expressions in both systems (Eqs. (9.6) and (9.12)) then using Eq. (9.9), it is straightforward to show that both representations for the density gradient are equivalent. The difference between both vanishes, as expected:

$$s(\mathbf{r})\int f(\mathbf{r}')\boldsymbol{\varepsilon}(\mathbf{r}')d\mathbf{r}' = s(\mathbf{r})\int f(\mathbf{r}')\sum_B \boldsymbol{\varepsilon}_B(\mathbf{r}')d\mathbf{r}' = s(\mathbf{r})\sum_B \mathbf{\Phi}_B = 0, \tag{9.13}$$

where $\sum_B \mathbf{\Phi}_B = 0$ since the sum of all forces acting on the nuclei vanishes, $\sum_B \mathbf{F}_B = 0$ [46].

9.4 The energy expansion in $E[N; v(\mathbf{r})]$ and $E[N; \{\mathbf{R}\}]$ representations

Two sets of energy derivatives have been collected for the use in the electronic energy expansion: the local functional derivatives over external potential $\delta/\delta v(\mathbf{r}')$ typical in the CDFT formalism, and the corresponding vector derivatives over atomic positions, $\nabla_B \equiv \partial/\partial \mathbf{R}_B$. The relations between these two types of derivatives have been presented first, and their much different nature has been emphasized. Derivatives in the $E[N; \{\mathbf{R}\}]$ representation are observables characterizing well-defined atoms and their links in a closed system. Direct relations between these physical derivatives and local derivatives represent an alternative to condensation of the local derivatives to atoms by their integration over an arbitrary chosen part of space. By this method, bonded atoms – the focus of all chemistry – may be endowed with an accurate physical measure of their changes in a reaction.

Both types of the energy derivatives are equivalent when calculated within the same system $N = const.$ or $\mu = const.$, and they must lead to the same energy change on disturbing the external potential by a displacement of atoms.

9.4.1 The roadmap linking the CDFT derivatives to the chemical observables

The whole body of the derivatives up to the third degree has been presented previously by the authors [36,37]. In Scheme 9.1 only those necessary to for

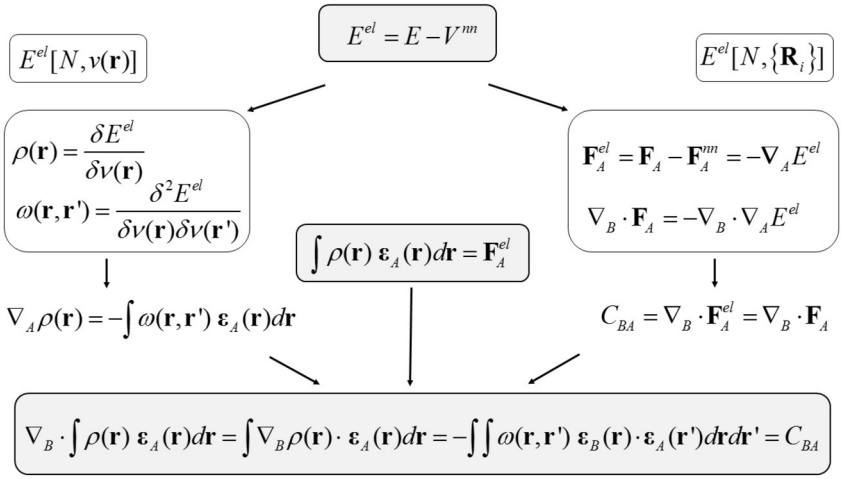

SCHEME 9.1 Relations between derivatives of the electronic energy in the local representation $E^{el}[N; v(\mathbf{r})]$ and the corresponding total energy derivatives in the nuclear coordinate representation $E^{el}[N; \{\mathbf{R}\}]$ for $N = const$. The H–F force on a nucleus is by definition $\mathbf{F}_A \equiv -\nabla_A E$ and $\mathbf{F}_A^{el} = -\nabla_A E^{el}$ stands for the electronic part thereof; C_{BA} is an element of the DF Connectivity Matrix, N is the number of electrons.

the energy expansion (2nd degree) have been collected, as they expose the most important feature of the vector analysis thereof, demonstrated in earlier work: the divergences of the nuclear repulsion forces vanish, i.e., $\nabla_B \cdot \mathbf{F}_A^{nn} = 0$ [46]. As a consequence, the second derivatives of energy in $E[N; \{\mathbf{R}\}]$ representation are equivalent to their counterparts calculated for the electronic energy in the CDFT closed system. Vector derivatives (divergencies) that form the DF connectivity matrix of the system $\underline{\underline{\mathbf{C}}}$ are all available directly by proper summation of the elements of Cartesian Hessian [46,77].

9.4.2 The DF connectivity matrix $\underline{\underline{\mathbf{C}}}$ vs the Cartesian Hessian $\underline{\underline{\mathbf{K}}}$

The two matrices may be presented in the atomic resolution as

$$\underline{\underline{\mathbf{C}}} = \begin{bmatrix} C_{AA} & C_{BA} & C_{CA} & \cdots \\ C_{AB} & C_{BB} & \cdots & \\ C_{AC} & \cdots & & \\ \cdots & & & \end{bmatrix} \quad \text{and} \quad \underline{\underline{\mathbf{K}}} = \begin{bmatrix} \underline{\underline{\mathbf{k}}}_{AA} & \underline{\underline{\mathbf{k}}}_{BA} & \underline{\underline{\mathbf{k}}}_{CA} & \cdots \\ \underline{\underline{\mathbf{k}}}_{AB} & \underline{\underline{\mathbf{k}}}_{BB} & \cdots & \\ \underline{\underline{\mathbf{k}}}_{AC} & \cdots & & \\ \cdots & & & \end{bmatrix}. \tag{9.14}$$

The Cartesian Hessian matrix ($\underline{\underline{\mathbf{K}}}$, $3n \times 3n$) of the second energy derivatives may be viewed as an ($n \times n$) block matrix where each $\underline{\underline{\mathbf{k}}}_{AB}$ block (3×3) is a pair-interaction matrix as exposed in the work by Seminario [83]. The full set of matrix elements between atoms A and B can be written symbolically as the

dyad of ∇_B and $\mathbf{F}_A$ vectors (see Appendix 9.A.3),

$$\underline{\underline{\mathbf{k}}}_{AB} \equiv [\nabla_B \otimes \mathbf{F}_A]. \tag{9.15}$$

Here $\mathbf{F}_A$ is total force including the n–n interactions, Eq. (9.15) may be separated into electronic and internuclear contributions, $\underline{\underline{\mathbf{k}}}_{AB} = \underline{\underline{\mathbf{k}}}^{el}_{AB} + \underline{\underline{\mathbf{k}}}^{nn}_{AB}$.

The elements of the DF connectivity matrix $\underline{\underline{\mathbf{C}}}$ are by definition the traces of $\underline{\underline{\mathbf{k}}}^{el}_{AB}$ blocks (cf. Scheme 9.1), or the dot-products of ∇_B and $\mathbf{F}_A$ vectors. It has been demonstrated by the authors in their preceding work, that the AB blocks of the nuclear interactions are traceless since $\nabla_B \cdot \mathbf{F}^{nn}_A = 0$ [46]. Hence,

$$C_{AB} = \nabla_B \cdot \mathbf{F}_A = Tr\underline{\underline{\mathbf{k}}}_{AB} = Tr\underline{\underline{\mathbf{k}}}^{el}_{AB} = \nabla_B \cdot \mathbf{F}^{el}_A. \tag{9.16}$$

9.4.3 The energy expansion

Expansion of the energy $E^{el}[N, v(\mathbf{r})]$ in a Taylor series has been recently reminded by Boisdenghien et al. in their study on the properties of the linear response function. When $N = \text{const.}$ (closed system), the expansion reads [16]

$$\Delta E^{el} = \int \rho(\mathbf{r})\Delta v(\mathbf{r})d\mathbf{r} + \frac{1}{2}\int\int \omega(\mathbf{r},\mathbf{r}')\Delta v(\mathbf{r})\Delta v(\mathbf{r}')d\mathbf{r}d\mathbf{r}' + \ldots \tag{9.17}$$

Here $\Delta E^{el} = \Delta E - \Delta V^{nn}$ stands for the electronic energy, exclusively. In the absence of external fields other than generated by the nuclei in the system, the change in the external potential $\Delta v(\mathbf{r})$ may be expressed with the displacements of the nuclei vectors ($\Delta\mathbf{R}_A$), by introducing the external electric field strength vectors $\boldsymbol{\varepsilon}_A(\mathbf{r})$ for each nucleus (cf. Appendix 9.A.1). Eq. (9.17) is transformed to a form with atoms clearly identified, namely

$$\begin{aligned}\Delta E^{el} = &-\sum_A \Delta\mathbf{R}_A \cdot \int \rho(\mathbf{r})\boldsymbol{\varepsilon}_A(\mathbf{r})d\mathbf{r} + \\ &+\frac{1}{2}\int\int \omega(\mathbf{r},\mathbf{r}')\sum_A\sum_B \{\Delta\mathbf{R}_A \cdot \boldsymbol{\varepsilon}_A(\mathbf{r})\}\left\{\Delta\mathbf{R}_B \cdot \boldsymbol{\varepsilon}_B(\mathbf{r}')\right\} d\mathbf{r}d\mathbf{r}'\end{aligned} \tag{9.18}$$

The integral within the first term represents the electronic part of the H–F force ($\mathbf{F}^{el}_A$, cf. Scheme 9.1). The combination of two dot-products of vectors (second term in Eq. (9.18)) may be regrouped. It is alternatively represented by the dyadic product $\left[\boldsymbol{\varepsilon}_A(\mathbf{r}) \otimes \boldsymbol{\varepsilon}_B(\mathbf{r}')\right]$ (the 3×3 matrix, cf. Appendix 9.A.3), or else, the order within the dot-products may be altered [84,85]:

$$\begin{aligned}&\{\Delta\mathbf{R}_A \cdot \boldsymbol{\varepsilon}_A(\mathbf{r})\}\left\{\Delta\mathbf{R}_B \cdot \boldsymbol{\varepsilon}_B(\mathbf{r}')\right\} = \\ &\quad = \Delta\mathbf{R}_A \cdot \left[\boldsymbol{\varepsilon}_A(\mathbf{r}) \otimes \boldsymbol{\varepsilon}_B(\mathbf{r}')\right] \cdot \Delta\mathbf{R}_B = \{\Delta\mathbf{R}_A \cdot \Delta\mathbf{R}_B\}\left\{\boldsymbol{\varepsilon}_A(\mathbf{r}) \cdot \boldsymbol{\varepsilon}_B(\mathbf{r}')\right\}\end{aligned} \tag{9.19}$$

where $\Delta\mathbf{R}_A$ and $\Delta\mathbf{R}_B$ are displacement vectors of atoms in the Cartesian system of coordinates. Considering Eq. (9.19) (last term), the double integral in Eq. (9.18) is transformed into the form containing an integral identical with the CDFT expressions for an element of the connectivity matrix C_{AA} or C_{BA}, as given in Scheme 9.1, respectively,

$$\Delta E^{el} = -\sum_A \Delta\mathbf{R}_A \cdot \mathbf{F}_A^{el} + \\ + \frac{1}{2}\sum_A \sum_B (\Delta\mathbf{R}_A \cdot \Delta\mathbf{R}_B) \int\int \omega(\mathbf{r},\mathbf{r}') \left\{\boldsymbol{\varepsilon}_A(\mathbf{r}) \cdot \boldsymbol{\varepsilon}_B(\mathbf{r}')\right\} d\mathbf{r}d\mathbf{r}'. \tag{9.20}$$

Eq. (9.20) represents the general expression for the electronic energy contribution associated with a virtual displacement of atoms in a system; the electronic force $\mathbf{F}_A^{el}$ does not vanish for a stationary state of a system,

$$\Delta E^{el} = -\sum_A \Delta\mathbf{R}_A \cdot \mathbf{F}_A^{el} - \frac{1}{2}\sum_A \sum_B (\Delta\mathbf{R}_A \cdot \Delta\mathbf{R}_B)\, C_{AB}. \tag{9.21}$$

An alternative formulation of this result may also be reproduced. The dyadic product (the second term in Eq. (9.19)) can be introduced into Eq. (9.18) (second term), yielding

$$\Delta E^{el} = -\sum_A \Delta\mathbf{R}_A \cdot \mathbf{F}_A^{el} + \\ + \frac{1}{2}\sum_A \sum_B \Delta\mathbf{R}_A \cdot \left\{\int\int \omega(\mathbf{r},\mathbf{r}') \left[\boldsymbol{\varepsilon}_A(\mathbf{r}) \otimes \boldsymbol{\varepsilon}_B(\mathbf{r}')\right] d\mathbf{r}d\mathbf{r}'\right\} \cdot \Delta\mathbf{R}_B. \tag{9.22}$$

By substituting $\underline{\underline{\mathbf{k}}}_{AB}^{el} = \int\int \omega(\mathbf{r},\mathbf{r}') \left[\boldsymbol{\varepsilon}_A(\mathbf{r}) \otimes \boldsymbol{\varepsilon}_B(\mathbf{r}')\right] d\mathbf{r}d\mathbf{r}'$, the classical result written with the Cartesian Hessian is obtained, namely

$$\Delta E^{el} = -\sum_A \Delta\mathbf{R}_A \cdot \mathbf{F}_A^{el} + \frac{1}{2}\sum_A \sum_B \left(\Delta\mathbf{R}_A \cdot \underline{\underline{\mathbf{k}}}_{AB}^{el} \cdot \Delta\mathbf{R}_B\right). \tag{9.23}$$

Eqs. (9.21) and (9.23) are identical, since the result for the product in parentheses (Eq. (9.23)) is

$$\Delta\mathbf{R}_A \cdot \underline{\underline{\mathbf{k}}}_{AB}^{el} \cdot \Delta\mathbf{R}_B = (\Delta\mathbf{R}_A \cdot \Delta\mathbf{R}_B)\, Tr\left(\underline{\underline{\mathbf{k}}}_{AB}^{el}\right). \tag{9.24}$$

Given Eq. (9.16) and $Tr\underline{\underline{\mathbf{k}}}_{AB}^{nn} = 0$, the final result may be formulated for the overall energy of the system as

$$\Delta E = -\sum_A \Delta\mathbf{R}_A \cdot \mathbf{F}_A - \frac{1}{2}\sum_A \sum_B (\Delta\mathbf{R}_A \cdot \Delta\mathbf{R}_B)\, C_{AB}. \tag{9.25}$$

The second term in the Taylor expansion for the energy may be formulated by means of the connectivity matrix (Eq. (9.25)), rather than by the Cartesian Hessian; it represents the vibrational energy ΔE_{vib}. For a system in equilibrium, the first term vanishes. The proof has been accomplished: the connectivity matrix represents a complete measure for the vibrational energy contribution to the energy of a system. By using the basic properties of the connectivity matrix $\sum_A C_{AB} = 0$ and $C_{AB} = C_{BA}$, this vibrational energy term has been transformed to a workable general expression (cf. Appendix 9.A.4)

$$\begin{aligned}\Delta E_{vib} &= -\frac{1}{2}\sum_A \sum_B (\Delta \mathbf{R}_A \cdot \Delta \mathbf{R}_B)\, C_{AB} = \\ &= +\frac{1}{2}\sum_A \sum_{B<A} |\Delta(\mathbf{R}_A - \mathbf{R}_B)|^2\, C_{AB} = \frac{1}{2}\sum_A \sum_{B<A} C_{AB}\, |\Delta \mathbf{R}_{AB}|^2 .\end{aligned} \tag{9.26}$$

Hence, the nondiagonal elements of the connectivity matrix indeed serve as the force constants for all A–B contacts in a system.

9.4.4 Atomic fragility modes

The result presented in the previous section points to the very important role of the DF Connectivity Matrix in describing the vibrational energy of molecules in atomic resolution. Diagonalization of the Cartesian Hessian is subject of the classical analysis and leads to the $3n - 6$ (or $3n - 5$) vibrational normal modes for a molecule (λ_α) and their frequencies [86,87]. Analogous procedure for the $\underline{\underline{\mathbf{C}}}$ matrix yields $(n - 1)$ modes, hereby referred to as the atomic fragility modes (Λ_ν) [77], $\underline{\underline{\mathbf{L}}}\underline{\underline{\mathbf{C}}}\underline{\underline{\mathbf{L}}}^T = \underline{\underline{\mathbf{\Lambda}}}$. While the normal modes (λ_α) represent the collection of independent oscillators (harmonic), the atomic modes (Λ_ν) describe somewhat condensed picture thereof. The DF Connectivity Matrix elements are cumulative force constants [46] (or effective, according to King [47]), referring to an atom trapped in the potential energy well, which is induced by the electron density function of the entire system.

The relation between these two solutions, the normal modes (λ_α) and the atomic modes (Λ_ν), is indirect, but has been implied by the frequency sum rule described by King and Wilson et al. [47,50]. In the framework of this present work, the sum rule reads

$$\sum_{\alpha}^{3n-6} \lambda_\alpha = \sum_{\nu}^{n-1} \Lambda_\nu, \tag{9.27}$$

where λ_α and Λ_ν stand for the eigenvalues of matrices $\underline{\underline{\mathbf{K}}}$ and $\underline{\underline{\mathbf{C}}}$, respectively. Eq. (9.27) exposes the difference between the two methods for analysis of a vibrating molecule, i.e., the normal modes and the atomic modes. Unlike the normal modes, the eigenvalues Λ_ν describe the electronic energy exclusively.

The number of the atomic modes $(n-1)$ is less than that of the normal modes $(3n-6)$, indicating that the atomic modes are physically realized by groups of normal modes. However, the eigenvalues for normal modes cannot be directly attributed to eigenvalues of specific atomic modes, as the nuclear energy of a system (V^{nn}) may not be divided between atoms. The crucial information on the reacting system is provided by the eigenvectors $\underline{\underline{\mathbf{L}}}$ associated with the eigenvalues (Λ_ν) of the DF Connectivity Matrix $\underline{\underline{\mathbf{C}}}$ [77]. The eigenvectors are normalized, hence the squares of atomic coefficient for a given mode, $\left(L_A^\nu\right)^2$, provide direct information on the involvement of atoms (A) in atomic modes (ν). Also $\left(L_A^\nu\right)^2$ reflects the role of individual atom in a particular, physically realistic vibration pattern affecting the electronic energy. This opens a novel observation point potentially valuable for a chemical reaction, namely observation of the variable role of displacement of individual atoms in disturbing the electronic energy of a whole system. The atomic eigenvalues have still the meaning of force constants, hence a collection of eigenvalues and eigenvectors calculated on a IRC reaction trajectory provide comprehensive information on an evolution of bonding interactions in a system and on the role of individual atoms therein.

9.5 Application to a chemical reaction

Formal analysis presented in Section 9.4 hints to the potential of the method, when it is applied to a chemical reaction. The energy formulas of Eqs. (9.25) and (9.26) remain valid for any fixed configuration of the nuclei, if the stationary electron density function is found by solving the Schrödinger equation (under Born–Oppenheimer approximation). Should that be a state of equilibrium (RS, TS, PS), the forces will vanish on every atom, $\left(\mathbf{F}_A^{el}+\mathbf{F}_A^{nn}\right)=0$. Otherwise, the first term in Eq. (9.25) is nonzero; nevertheless, the second term preserves its meaning of the sum of virtual contribution to the vibrational energy from each particular contact in the system.

The IRC method provides the firm ground for this matter: the stationary electron state is granted at each step of the reaction path. The reaction progress parameter ξ, as defined in the IRC formalism, offers a tool for extending the mathematical analysis. Every state on a reaction path represents a well-defined configuration of atoms: at each step forward along the path defined by the increase of the reaction progress by $\Delta\xi$, the position of an atom varies by $\Delta\mathbf{R}_A=(d\mathbf{R}_A/d\xi)\,\Delta\xi$. Moreover, the $\mathbf{R}_A(\xi)$ dependence is limited to the linear function, according to the computational rigor on IRC [74,75]. Hence, each step forward on the reaction path may be used to diagnose the vibrational properties of the given configuration of atoms.

The observation of gradual changes of the force constants in a system on the subsequent reaction steps on the way from reagents (RS) to products (PS) contains valuable information on the mechanism of this reaction, especially as the present analysis is focused on the electronic energy contributions to bonds. In our earlier work we have studied the evolution of H–F forces along IRC path and

their the projection onto the reaction coordinate [88]. The second energy derivative over the reaction progress (the reaction force constant) has been advocated by Politzer et al. [89,90]. Both derivatives have also been formulated in the atomic resolution for use for the chemical purposes [75]. The formal analysis in Section 9.4.3 has provided the new perspective to this approach, by proving the electronic character of the second derivative over displacement of atoms, when calculated on the ground of the vector analysis, and also, by demonstrating the additive character of contributions from all bond/contacts to the vibrational energy of a system.

9.5.1 The third energy derivative over reaction progress

The third derivative of energy over reaction progress (an anharmonicity parameter) has not yet been analyzed as such. Our novel approach allows for a natural description of the anharmonic effects with the use of the Reaction Fragility concept $a_\xi = d(Tr\underline{\underline{\mathbf{C}}})/d\xi$ [52] that has served as a leverage for the idea a of the Reaction Fragility Spectra [46].

Eqs. (9.25) and (9.26) allow identifying all three energy derivatives in the energy expansion with respect to ξ and discovering their informative potential for a chemical reaction. The Taylor expansion for the energy function $E(\xi)$ reads

$$-\Delta E(\xi) = F_\xi \Delta\xi + \frac{1}{2} K_\xi \Delta\xi^2 + \frac{1}{6} A_\xi \Delta\xi^3. \tag{9.28}$$

The physical meaning of all three terms in this energy expression has been well founded: the first represents the reaction force work [91], the second stands for the vibrational energy (harmonic), and the last anharmonic term describes directly the actual change of the bond structure – the chemical change. The derivatives in Eq. (9.28) can be expressed in the atomic resolution, using the result presented in Eq. (9.25) for the total energy. By using the natural substitution $\Delta\mathbf{R}_A = (d\mathbf{R}_A/d\xi)\,\Delta\xi$, the reaction force in Eq. (9.28) is equivalent to the formerly presented result for projection of the HF forces onto the reaction coordinate [75],

$$F_\xi = -\sum_A \left(\mathbf{F}_A^{HF} \cdot \frac{d\mathbf{R}_A}{d\xi} \right). \tag{9.29}$$

The second derivative (K_ξ constant) in atomic resolution will be extracted from the second term the expansion in Eq. (9.25). Thanks to the applied vector formulation, it has been proved to be of an electronic nature only, which makes it superior for the chemical analysis over the conventional reaction force constant. Moreover, K_ξ can be related to the DF Connectivity Matrix elements C_{AB} rather that to the Cartesian Hessian elements by using the result for the second term proved with Eq. (9.26) (the transformation of the product of vectors $d\mathbf{R}_A/d\xi$

and $d\mathbf{R}_B/d\xi$ is holding; see Appendix 9.A.4):

$$K_\xi = -\sum_A \sum_{B<A} D_{AB} C_{AB} \quad \text{where } D_{AB} = \left| \frac{d\mathbf{R}_{AB}}{d\xi} \right|^2. \tag{9.30}$$

For the sake of brevity, the distance factor for bonds has been introduced as D_{AB}. The global third energy derivative over the reaction progress will also be sought for in the vector formulation. The reaction anharmonicity $A_\xi = dK_\xi/d\xi$ must be calculated when observing the local linearity condition on IRC, $d^2\Delta\mathbf{R}_A/d\xi^2 = 0$. Hence,

$$A_\xi = \frac{dK_\xi}{d\xi} = -\sum_A \sum_{B<A} D_{AB} \frac{dC_{AB}}{d\xi} = \sum_A \sum_{B<A} D_{AB} a_\xi^{AB}. \tag{9.31}$$

Notably, this result for the reaction anharmonicity A_ξ in Eq. (9.31) is entirely localized in bonds/contacts between atoms. The new quantity, $a_\xi^{AB} = -dC_{AB}/d\xi$, has been introduced in previous works from this laboratory under the name "bond fragility" [72]. The relation of the bond fragility to the physical measures of anharmonicity can be demonstrated (Eq. (9.32)) with the atomic anharmonicity vectors introduced and discussed in our previous work [37], namely $\boldsymbol{a}_{ZAB} \equiv \nabla_Z C_{AB} = dC_{AB}/d\mathbf{R}_Z$, as

$$a_\xi^{AB} = -\frac{dC_{AB}}{d\xi} = -\sum_Z^{atoms} \boldsymbol{a}_{ZAB} \cdot \frac{d\mathbf{R}_Z}{d\xi}. \tag{9.32}$$

The variation of the energy parameter K_ξ along a reaction path reflects the ongoing modification of internal structure of bonds in a reacting system – a chemical change induced by a reaction, the A_ξ derivative reports the intensity of this effect. There are, however, two sources of change in K_ξ and A_ξ with $\Delta\,\xi$, clearly distinguishable in Eqs. (9.30) and (9.31): first, the simple shift of atoms resulting in the modification of their distance $d\mathbf{R}_{AB}/d\xi$, and second, the modification of the electronic nature of the system sensed by the DF Connectivity Matrix elements C_{AB}. The latter effect is an essence of the A_ξ parameter representing a sum of the bond fragilities a_ξ^{AB} weighted by the corresponding change in the distance factor between atoms, $D_{AB} = |d\mathbf{R}_{AB}/d\xi|^2$. The role of DF Connectivity Matrix has been fully exposed because the variations of its elements described by the bond fragilities a_ξ^{AB} have now been proved to indeed reflect the real chemical changes in a system.

9.5.2 Relation to the local modes (adiabatic internal modes)

An anticipated, indirect relation between anharmonicity phenomenon and a chemical reaction has also been present in the unified reaction valley approach (URVA) by Kraka and collaborators [92]. Their description of the chemical reaction mechanism is derived from the evolution of the normal modes (independent

oscillators) along the IRC reaction path by the transformation to the diagonal force constant matrix $\underline{\underline{\mathbf{K}}}$. The introduction of the adiabatic curvature coefficients tentatively assigned to bonds, as developed by these authors, allows replacing the need of anharmonicity discussion. The reaction path is described by the set of harmonic oscillators with a different force constant at each step [64,93]. One distinguished mode follows the reaction path (at $\xi = 0$, it is a transition state mode), the other $3N - 7$ modes are perpendicular to the reaction path and to each other. These normal modes undergo variation along the IRC path; the nonadiabatic curvature coefficients provide information on which mode drives the reaction and the Coriolis coefficients show which modes tend to exchange energy with each other. The authors have presented an ingenious approach to localization of the normal modes into a predefined molecular fragment: "*the fragment motion is considered as a motion being obtained after relaxing all parts of the vibrating molecule but the fragment under consideration*" [71]. The term local modes has been adopted for these adiabatic internal coordinate modes. The proof has been presented that the local stretching force constant for an AB entity reflects the intrinsic strength of the bond/interaction between atoms A and B [71]. The local stretching force constants have been claimed to represent the "*universal measure of the intrinsic strength of a chemical bond based on vibrational spectroscopy* [71]"; the proof is based on the Morse model.

The Reaction Fragility (RF) method, as documented in this present work, has common root with the local mode methodology by Kraka et al., that is, the Hessian matrix calculated for the consecutive steps along IRC. The firm theoretical background supports the RF method: the complete neglect of the internuclear interactions is possible by the Laplace law, and the DF Connectivity Matrix provides the characteristics of any system of interacting atoms, including the specific collection of electronic stationary states along an IRC. By the CDFT interpretation for the elements of the DF Connectivity Matrix (Scheme 9.1), they have been endowed with the exact, universal, and unconditional relation to the electron density via the linear response function $\omega(\mathbf{r}, \mathbf{r}') = \left[\delta\rho(\mathbf{r})/\delta v(\mathbf{r}')\right]_N$. They provide a definite measure of the electronic strength of all contacts between atoms in their natural environment in a molecule. Moreover, since the bond breaking and forming is primarily based on the redistribution of the electron density, this is immediately seen with the Reaction Fragility method, by observation of the derivatives of the corresponding DF Connectivity Matrix elements over reaction progress along a reaction path. This result could have been approximated by the original URVA method for a specified molecular fragment only.

The important practical advantage of the Reaction Fragility method rests on simplicity of its numerical procedure: computation of the full Hessian matrix is the condition both necessary and sufficient for its implementation. Whenever a procedure exists for obtaining branches of the IRC path, also the Hessian for each branch will be obtained straightforwardly, and the Reaction Fragility monitoring is possible for each branch of the bifurcation. The Reaction Fragility

method also is not vulnerable to the trajectories of the second-order transition states with two negative frequencies. For the Reaction Fragility method, the reaction path is just a trajectory connecting points of variable molecular geometry, and yet the principal advantage of the method comes from the fact that it is exact. Discovering a relation between the local modes based on vibrational spectroscopy (URVA), and the atomic modes (RFM), represents a challenging task for further studies.

9.6 Example: the internal proton transfer in formamide

Following the formal analysis presented in Sections 9.4 and 9.5, the practical consequences of the diagonalization of the DF connectivity matrix have been analyzed. The atomic modes have been tested as a tool for tracing a role of atoms in evolution of a system on a reaction path for the proton transfer reaction in formamide. Also, the contributions of individual bonds/contacts to the vibrational energy of and to anharmonicity parameter of this reacting system have been tested.

9.6.1 Computational details

Numerical results for the elements of the DF connectivity matrix have been obtained from calculation of the IRC energy profile by the standard procedure at the MP2 level using the 6-311++G($3df$,$3pd$) basis set and the Gaussian 09 code [94]. The internal proton transfer reaction has been selected as an example, the preliminary data for the diagonalization of the connectivity matrix have already been reported for this molecule (in RS, TS, and PS only) [77,95]. H_2N–CHO molecule has been considered in the planar configuration, as established in the former works [95]. The TS structure has been identified by means of the QST2 algorithm and verified with the frequency calculation for the normal vibrational modes. The reaction progress parameter (ξ) has been calculated in the mass-weighted coordinates at 105 points over reaction path covering the range ($-2.90 < \xi < +2.50$). The Cartesian Hessian has been calculated for each single point on the trajectory using the geometry of the structures on the IRC; the elements of the DF connectivity matrix have been calculated by proper summation of Cartesian Hessian elements [96], $C_{AB} = k_{Ax,Bx} + k_{Ay,By} + k_{Az,Bz}$.

The DF connectivity matrices $\underline{\underline{\mathbf{C}}}$ calculated for points on IRC have been diagonalized separately by the numerical NumPy (v.1.17.2) method available online [97–99]. To reassure the correct identification of eigenvectors with eigenvalues (Λ_v), calculated separately at every point on the reaction path, an independent procedure has been executed with the algorithmic method, for three characteristic points, namely RS, TS, and PS [100]. This provided a test for proper identification of atoms in normalized eigenvectors resulting from the numerical procedure - L^2_{vA} coefficients corresponding to the eigenvalues Λ_v. The individual functions $\Lambda_v(\xi)$ and $L^2_{vA}(\xi)$ have been sorted out separately from the

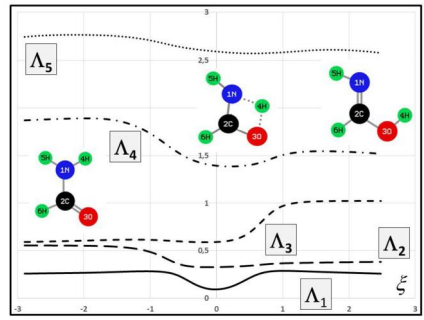

FIGURE 9.1 Eigenvalues of the DF connectivity matrix [Λ_v in Hartree/(Bohr)^2] variable on IRC (ξ) for the internal proton transfer reaction in formamide H_2N–CHO.

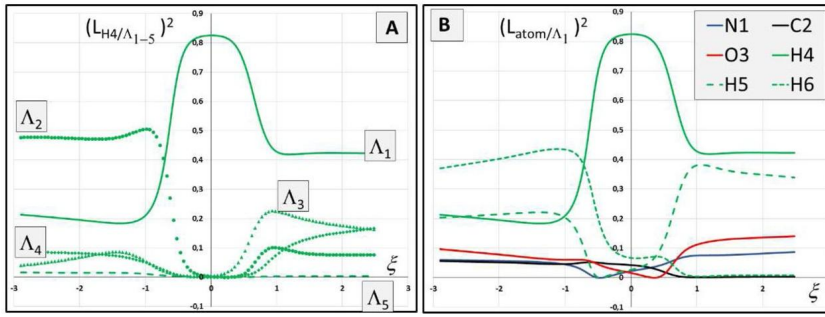

FIGURE 9.2 The squares of the normalized eigenvector coefficients variable along the reaction path for the internal proton transfer reaction in H_2N–CHO molecule: (A) The squares of eigenvector coefficients for the mobile H4 atom in all five atomic modes. (B) The squares of eigenvector coefficients for all atoms in the lowest Λ_1 atomic mode.

corresponding collections of numerical data (Λ vs ξ and L^2 vs ξ), as smooth (differentiable) curves accordingly. The eigenvalues for the DF connectivity matrix along IRC have been shown in Fig. 9.1. All numerical data have been presented in the atomic units: C_{AB} [Hartree/(Bohr)^2], ξ [(amu)$^{1/2}$Bohr].

9.6.2 Characteristics of the atomic fragility modes

In order to visualize the normalized eigenvectors, two types of diagram may be used, by collecting them by atoms or by the modes. Both types of diagram have been depicted in Fig. 9.2(A) for the most active atom (H4) and the lowest atomic fragility mode (Λ_1). Eigenvectors for H4 and atoms within the same atomic fragility mode (lowest energy) have been shown in Fig. 9.2(B). The normalized eigenvector coefficients for other atomic modes and for other atoms in the system have been collected in Figs. 9.3 and 9.4, respectively.

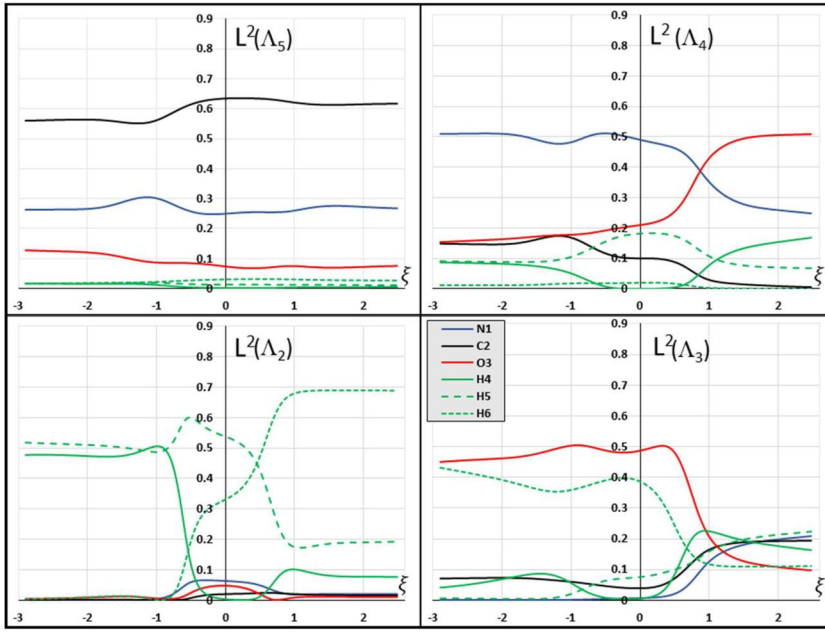

FIGURE 9.3 The squares of the normalized eigenvector coefficients of atoms in the eigenvectors for atomic modes Λ_2–Λ_5 in formamide, along the IRC for the internal proton transfer reaction.

9.6.3 Vibrational energy distribution in bonds

Eq. (9.26) allows for attribution of the vibrational energy to bonds and contacts in the reacting system. This has been envisaged by calculating the K_ξ parameter (Eqs. (9.28) and (9.30)) traced along the IRC reaction path and the principal results have been presented in Fig. 9.5. The vibrational energy contribution has been dominated by the bonds undergoing changes N1- - -H4 and O3- - -H4 (Fig. 9.5(A)). However, the method has been sufficiently sensitive as to discover even the minute variations in other bonds and contacts playing a role in this reaction (Fig. 9.5(B)).

While no results for this same reaction have been available in order to judge the efficiency of the present method, the general feature of the characteristics in Fig. 9.5 may be compared to the curvature diagrams reported by Kraka and Cremer for the similar proton transfer reaction, namely S- - -C(H)OH $\rightarrow$ HSC(H)- - -O [92]. The scalar curvature characteristics for bonds reported in this work are dominated by the O–H bond cleavage at the reaction onset ($\xi \cong -1$), and by the S–H bond formation peak in the reaction decay ($\xi \cong 1$). The analogy to the shape, location, and role of the N1–H4 and O3–H4 curves in Fig. 9.5(A) is striking, and calls for formal analysis of the relevance between the two methodologies for monitoring reaction progress.

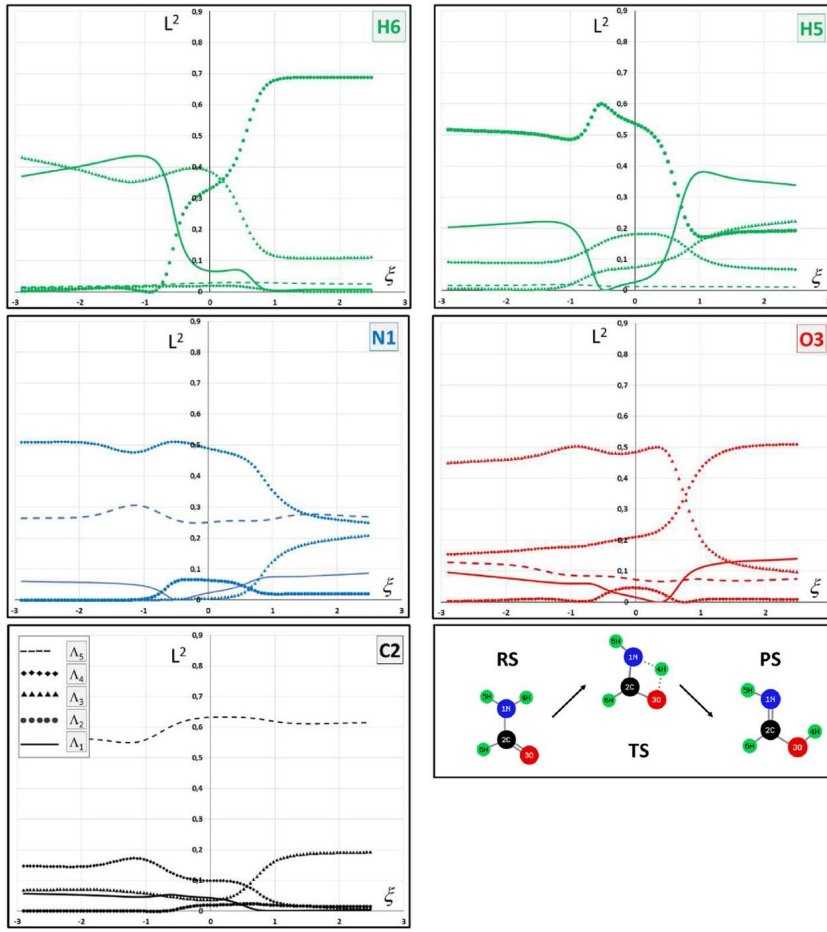

FIGURE 9.4 The squares of the normalized eigenvector coefficients of atoms in H_2N–CHO molecule for all atomic modes (Λ_1–Λ_5) along the IRC for the internal proton transfer reaction. The uniform style of lines for the atomic modes has been indicated on the diagram **C2**. For H4, consult Fig. 9.2(A).

9.6.4 Anharmonic parameter A_ξ and major contributions from bonds/contacts

The anharmonicity parameter for the reaction has been calculated according to Eq. (9.31). Also, the individual contributions from all bonds and contacts have been calculated; the major contributions have been collected in Fig. 9.6.

The next highest contribution from a bond (H4–H6) was by one order of magnitude smaller than the lowest contribution envisaged in Fig. 9.6 (H5–H4 contact). The character of curves for the two bonds undergoing the change in the proton transfer reaction (N1–H4 and H4–O3) is entirely defined by the cor-

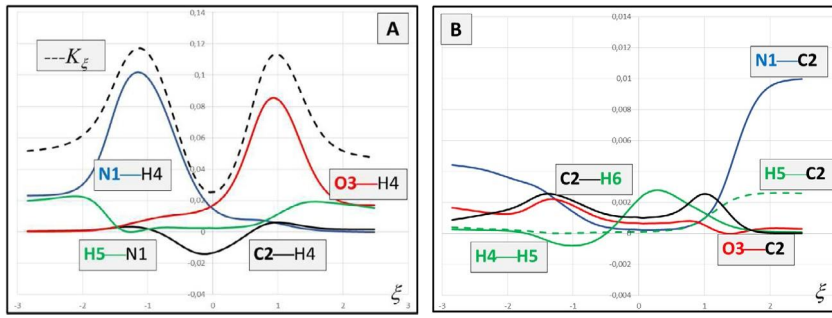

FIGURE 9.5 Major (A) and minor (B) contributions from bonds and/or contacts to the vibrational energy measured by the bond components to K_ξ constant (Eq. (9.30), in a.u.), along the reaction path for the internal proton transfer in H_2N–CHO. For the sake of clarity, the scale of the ordinate axis in Fig. 9.5 (B) has been expanded (10×).

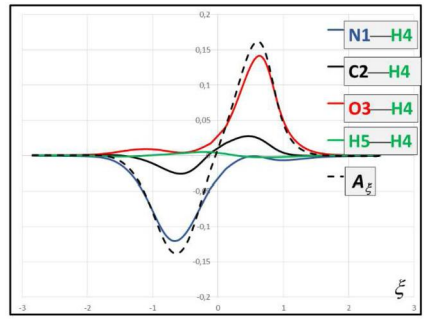

FIGURE 9.6 Contributions from bonds and contacts to the global anharmonicity parameter (A_ξ, Eq. (9.31), in a.u.) along the reaction path for the internal proton transfer in H_2N–CHO.

responding bond fragility spectra (a_ξ^{AB} vs ξ), as reported in previous work [95]. The relatively high contributions to overall anharmonicity parameter A_ξ from the two nonbonding contacts in the system (H4–C2 and H4–H5) is an interesting novel discovery in this reaction.

9.6.5 Reaction fragilities for atoms and bonds

The principal atomic and bond fragilities for this system, defined as $a_\xi^A = dC_{AA}/d\xi$ and $a_\xi^{AB} = -dC_{AB}/d\xi$, respectively, have already been presented for the reaction center, i.e., for the proton exchanging atoms [95]. It is now helpful to recall the fragilities for all atoms in the system (9.6) as well as for all their possible contacts (9.15), as they play crucial role in calculation of the anharmonicity parameters for the reaction A_ξ and its contributions. Since the atomic fragilities represent a sum of fragilities calculated for all bonds/contacts of each atom $a_\xi^A = \sum_B a_\xi^{AB}$, it is now possible to detect the role of even minute disturbances induced to bonds by the reaction. The diagrams in Figs. 9.7–9.11 have

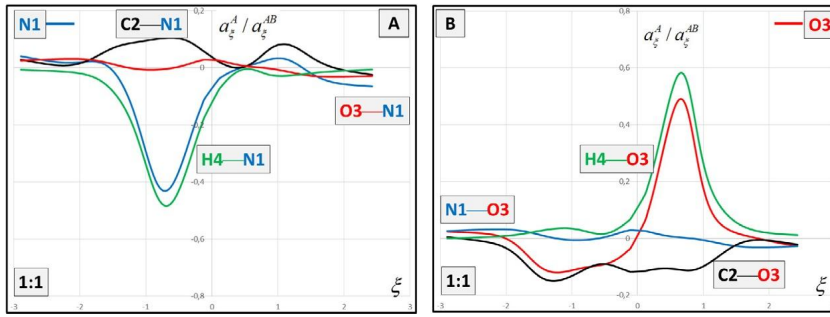

FIGURE 9.7 Calculated reaction fragilities (in a.u.) for atoms N1 (A) and O3 (B) and for their bonds/contacts along the reaction path for the internal proton transfer in H_2N–CHO. The bond fragilities for weak interactions of remaining atoms with N1 and O3 are shown on the diagrams for the respective partners in Fig. 9.8–9.11.

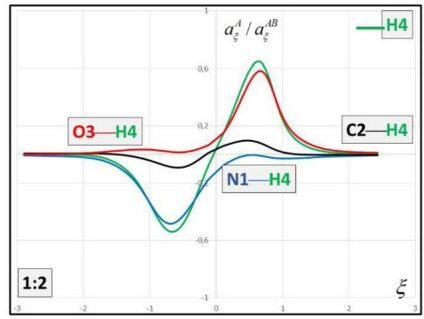

FIGURE 9.8 Calculated reaction fragility (in a.u.) for H4 atom and its bonds/contacts along the reaction path for the internal proton transfer in H_2N–CHO. Note the contraction of the scale on the ordinate axis by 1:2, with respect to the basic scale in Fig. 9.7 for N1 and O3 atoms.

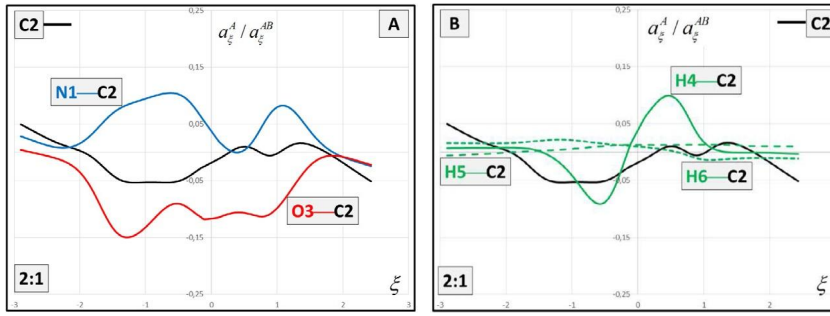

FIGURE 9.9 Calculated reaction fragility (in a.u.) for C2 atom and its bonds/contacts along the reaction path for the internal proton transfer in H_2N–CHO. Two group of atoms have been separately shown in the diagram for the sake of clarity as A and B. Note the expansion of the scale on the ordinate axis by 2:1, with respect to the basic scale in Fig. 9.7 for N1 and O3 atoms.

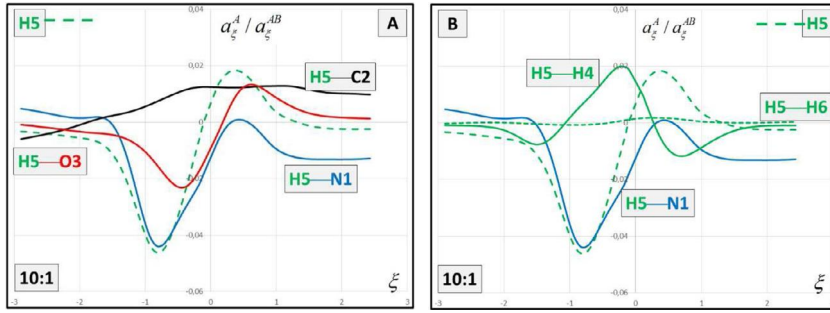

FIGURE 9.10 Calculated reaction fragility (in a.u.) for H5 atom and its bonds/contacts along the reaction path for the internal proton transfer in H_2N–CHO. Two group of atoms have been separately shown in the diagram for the sake of clarity as A and B. Note the expansion of the scale on the ordinate axis by 10:1, with respect to the basic scale in Fig. 9.7 for N1 and O3 atoms.

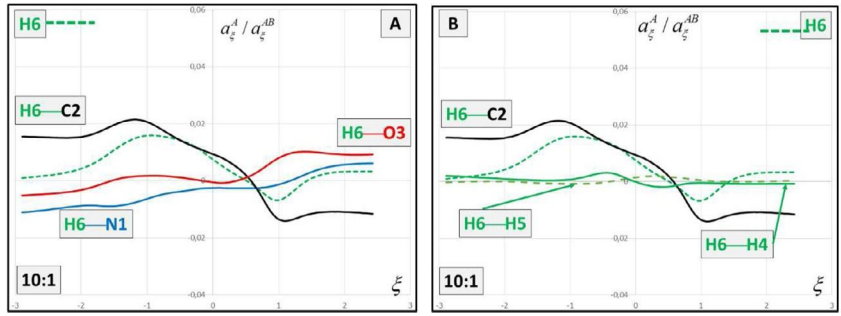

FIGURE 9.11 Calculated reaction fragility (in a.u.) for H6 atom and its bonds/contacts along the reaction path for the internal proton transfer in H_2N–CHO. Two group of atoms have been separately shown in the diagram for the sake of clarity as A and B. Note the expansion of the scale on the ordinate axis by 10:1, with respect to the basic scale in Fig. 9.7 for N1 and O3 atoms.

been segregated by atoms, hence the curves for the bond fragilities of some atoms have been repeated. The strong interactions for bonds have been separated from the weak ones for contacts and the ordinate axis has been adjusted separately, with the scaling factor marked on each diagram.

9.7 Discussion: quantitative monitoring of a chemical reaction

Two observations have been demonstrated for the specific model reaction of internal proton transfer in formamide, selected as an instructive example for assessing the method of computational monitoring atoms and bonds in reactions: (i) the novel atomic fragility modes representing the potential tool for evaluation the consequences of the structural modification brought about by the reaction, (ii) the direct quantitative information on bond evolution provided by

the fragility spectra with the anharmonicity parameters calculated on the reaction path.

9.7.1 The role of atoms for the atomic fragility modes

The concept of the atomic vibrational modes opens a novel, original observation point for chemical reactions. It is clear in Fig. 9.1 that all atomic modes are subject to change with regrouping of atoms. The lowest and presumably dominating atomic mode (Λ_1) is affected by the reorganization in the narrow range near TS ($-0.8 < \xi < 0.8$), in a typical, symmetric fashion with a minimum at TS. On the contrary, the high energy mode (Λ_5) is only slightly affected by the reaction, its gradual change covers the broadest range of the process ($-1.5 < \xi < 2.5$). The impact of the reaction on the intermediate energy modes (Λ_2, Λ_3, Λ_4) is significant, though rather unexpected. The energy of the (Λ_2) mode is considerably higher than (Λ_1) mode near the reaction onset (Fig. 9.1). The energy of (Λ_2) rapidly decays by ca. 30% at the point where the changes in (Λ_1) begin. The reverse phenomenon is observed for (Λ_3): its energy rises sharply by ca. 60% at the endpoint of the minimum at (Λ_1). The evolution of (Λ_2) and (Λ_3) modes clearly indicates their active role in the reaction. Modification of the high energy mode (Λ_4) is remarkably large and broad, covering the range ($-1.5 < \xi < 1.5$), suggesting a minor change of rather strong bonds. Quite interestingly, the TS point seems to be significant mark for the (Λ_1) mode only.

The above observation can be elucidated only by monitoring the participating atoms for each mode, the valuable result of this present work. Despite small number of atoms participating in the chosen reaction, the distinction of atoms into clearly separated groups is possible, with regard to their participation in the reaction events, as understood with chemical intuition: (i) the mobile atom H4, (ii) the affected atoms N1, H5, O3, and (iii) the spectator atoms C2, H6.

The squares of the normalized eigenvector coefficients for atoms provide the much wanted information as they disclose the effect of switching atoms between the modes, as the reaction proceeds. In the lowest energy mode (Λ_1), the mobile atom H4 has been found dominating in the vicinity of the TS point (Figs. 9.2(A) and 9.2(B)) as expected. Its role in the structure of this mode in the initial and final stages of the process is different. Near the RS state, the H6 atom is a dominant of this mode; its role vanishes entirely near TS (Fig. 9.2(B)). The H5 atom participation in (Λ_1) mode, initially nearly as high as the one of H4, falls down to zero at TS, then rises sharply, to meet the level of H4 at the end of the process, with equal share in this mode (ca. 40%). The heavy atoms appear to rest merely as spectators to this atomic mode.

The (Λ_2) atomic mode is also characterized mainly by the participation of protons, (Fig. 9.3, $L^2(\Lambda_2)$), with the significant, but small, maximum for the N1, O3 atoms, and to some extent also C2 atom around TS. At the initial stage, H4 and H5 atoms contribute equally to (Λ_2) mode, in the similar manner as they do in (Λ_1), but there is no share of H6 here. There is striking alteration of the

structure of this mode in its way to PS: at the end of the process, the H6 atom will dominate (70%). The initial symmetry in the contributions from H4 and H5 atoms and unique position of H6 atom in two lowest atomic modes is in harmony with the chemical character of the formamide molecule.

In the initial stage (RS), the (Λ_3) mode is close the (Λ_2), but its structure is considerably different (Fig. 9.3, $L^2(\Lambda_3)$). This mode involves initially the -CHO group of the molecule with only H6 and O3 atoms playing a role, until past the TS state (ca. $\xi \cong 1$). At this final point, contributions from O3 and H6 atoms are reduced to by 60% and they are replaced by H4, N1 and C2 atoms in roughly equal shares. The effect of the reaction is fully exposed by this change: the initially isolated –CHO group has been transformed to the coupled - - -N=CHOH entity.

The structure of the (Λ_4) atomic mode observed in Fig. 9.3, $L^2(\Lambda_4)$ well explains the remarkable change in the reaction and the broad range of bond modification along the reaction path. At the initial stage (RS) the mode characterizes the N–C–O skeleton, with N1 atom strongly dominating. This will not change substantially until towards the end of the reaction (ca. $\xi \cong 1$) where the O3 atom takes the lead, the contribution from C2 vanishes (C2 atom switches to Λ_3 mode, see above) and H4 atom joins the band, –N–C–OH. Further, (Λ_4) is the highest atomic mode where the reaction events have been marked: they are hardly noticed in the (Λ_5) atomic structure in Fig. 9.3, $L^2(\Lambda_5)$.

The variations of the atomic contributions to the eigenvectors calculated for the atomic modes as described above reveal their role in the process even better, when they are grouped by atoms, rather than by the modes. This has been shown in Fig. 9.4 for the skeleton atoms, in addition to Fig. 9.2(A) drawn for the moving H4 atom separately.

The panorama of atomic participation in the eigenvectors presented in Fig. 9.4 provides very instructive picture of the reaction mechanism. First, it becomes evident that the hydrogen atoms (H5, H6) serve as sensors for the actual changes introduced along the reaction path, even if they do not play directly a role in this process. Drifting H4 away from the N1 nitrogen is dramatically sensed by H5 and H6 atoms; docking H4 at O3 is manifested sharply by the distant H6 atom. Two heavy atoms (N1, C2) do not show dramatic alternation in their involvement in any of the atomic modes, despite the evident changes in their bond structure, that is,

$$H_2N–C(H)=O \rightarrow HN=C(H)–OH.$$

The N1 and C2 atoms participate with the considerable contribution only in the highest energy modes (Λ_4, Λ_5); the significant role of O3 atom for (Λ_3) mode marks clearly its active role for the reaction. The role of H5 and H6 atoms in the lowest atomic modes (Λ_1, Λ_2) could hardly be noticed by other observation methods.

9.7.2 Contributions from bonds/contacts to the vibrational energy

Quantitative parameters K_ξ and A_ξ calculated for the reaction path open a chance for new characterization of contacts between atoms in a system undergoing a reaction, by testing the stepwise evolution of their contributions to the vibrational energy along the way. Unlike the atomic and bond parameters describing inherent properties of a stationary system (e.g., C_{AA}, C_{AB}), the bond contributions to K_ξ and A_ξ report the energy required to make a step on the "optimal" path from reactants to products.

Contributions to the vibrational energy demonstrated in Fig. 9.5(A) indicate that at the initial RS state, most of the energy change is localized in the NH_2 group, and it is distributed in nearly equal parts between N1–H4 and H5–N1 bonds, with a small admixture from N1–C2 bond (Fig. 9.5(B)). The situation is only partially reversed in the final PS state: the energy change is localized largely in H4–O3 bond, however, the share of N1–H5 bond is recovered, after falling to zero near TS. The N1–C2 skeleton bond follows this trend, reaching at PS the level considerably higher than it has been at RS (Fig. 9.5(B)), as its formal bond order is increased. The nonbonding contact between C2 atom and the moving proton H4 must somehow play a role in the process (Fig. 9.5(A)), as it seems to introduce an element of stiffness to the system, considerably decreasing the vibration energy around TS. Otherwise, the skeleton atoms play little role in the process, with O3–C2 bond barely sensing the events (Fig. 9.5(B)), despite evident decrease of its formal bond order; the impact of the process on the C2–H6 bond is larger. Among the noticeable variation in Fig. 9.5, the H4–H5 contact deserves mentioning: it is loosened at the reaction onset, and it is recovered, somewhat unexpectedly, in the TS region as if another link between two atoms were created even before PS.

The meaning of the reaction anharmonicity curves A_ξ and the bond contributions thereto in Fig. 9.6 is less intricate than of the force constants in Fig. 9.5. High values of this parameter are convincingly associated with the running process of bond alternation in a system. It may be bond rupture (negative values) or bond creation (positive values). Significant values of the bond components reported in Fig. 9.6 are only few – apparently, the reaction is dominated by the N1–H4 bond breaking and O3–H4 bond creation. All noticeable contributions from bonds to A_ξ involve the links of H4 atom with all but the isolated H6 atom. The role H5–H4 contact, though marginal in this process, confirms the role of protons, being potential sensors for the electronic process nearby.

In order to complete the analysis of K_ξ and A_ξ derivatives, it is instructive to appraise the role of the distance factor $D_{AB} = |d\mathbf{R}_{AB}/d\xi|^2$ in Eqs. (9.30) and (9.31). It contains valuable information on the degree and direction of change in bond distances on the subsequent reaction steps, even though it is determined with the limitation of the IRC reaction path. The characteristic features of this factor have been illustrated by the sample diagrams (Fig. 9.12). The D value tends to be nearly constant in the distinctly separated regions, with the borderlines for the central TS region ca. $(-1.5 < \xi < 1.3)$; D_{AB} for all contacts

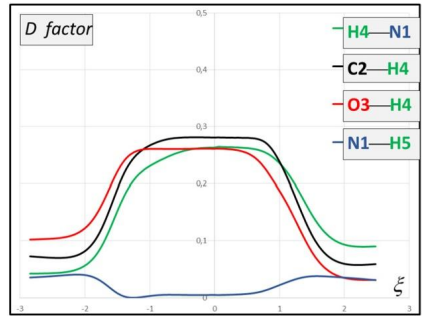

FIGURE 9.12 The distance factors $D_{AB} = |d\mathbf{R}_{AB}/d\xi|^2$ [a.u.] in Eqs. (9.30) and (9.31) for the selected bonds variable with the internal proton transfer in NH_2–CHO.

involving the mobile H4 atom distinctly increase in the central region, D_{AB} for other contacts are all negligibly small and slightly decreasing around TS; only one, most significant representative of this group has been brought to the picture (N1–H5, Fig. 9.7).

9.7.3 Sensitivity of the bond fragility analysis

The bond fragilities presented in Figs. 9.7–9.11 fall into three separate categories. The first represents the bonding interactions, considerably altered by the process: H4–N1, H4-O3 (Figs. 9.7 and 9.8). They show strong maxima/minima in their fragilities that dominate the change in the fragility of respective partner atoms and indicate the critical points on the reaction path, where the process driving the reaction really occurs. The striking similarity between the anharmonicity diagram for the active bonds (Fig. 9.6) and their bond fragilities (Fig. 9.8) proves the leading role of a_ξ^{AB} over D_{AB} factor in Eq. (9.31).

To the second group belong the bonds of considerably smaller fragilities (ca. by a factor of 1/5), but still indicating explicit participation in the electron exchange in the reaction: C2–N1 and C2–O3 (Fig. 9.7). Interesting information can be clearly deduced from Fig. 9.9(A): breaking the H4–N1 bond (Fig. 9.7) is associated with increase of the C2–N1 bond order for a moment, while O3–C2 bond suffers a parallel decrease (Fig. 9.9(A)). It is rather unexpected that the H4–C2 nonbonding contact also falls into this category, this contact too is broken at the initial phase of the reaction (Fig. 9.9(B)) and is restored as soon as the H4–O3 bond is formed (Fig. 9.8). Surprisingly, the H4–C2 bond share in the vibrational energy of the system appears to be negative for this bond in the TS region (Fig. 9.5(A)). The C2–N1 bond gains more strength near the end of the process (Fig. 9.7(A)), while the C2–O3 bond does not (see Fig. 9.7(B)): the well-understood chemistry of this process is formidably illustrated by the above diagrams inasmuch as C2–N1 and C2–O3 bonds are considered. On the other hand, the nonnegligible interaction between the moving proton H4 and C2 atom

is an intriguing discovery of the method. The contradictory changes around C2 atom explain the flat curve for the fragility of this atom (Fig. 9.9).

The third group of bond fragility curves incorporate the remaining bonds and contacts in the system; they all are clearly described, despite being by an order of magnitude smaller that the former. The H5–N1 bond (Fig. 9.10(A)) and H6–C2 bond (Fig. 9.9(B)) belong to this category. The former is clearly undermined by the process in the initial phase (Fig. 9.10(A)), so is the latter, but at the end of the process (Fig. 9.11(B)). Almost as strong a change as for these two bonds is observed for the H5–H4 contact (Fig. 9.10(B)) building up and H5–O3 contact falling dawn (Fig. 9.10(A)), despite the shortening the N1–H5 contact clearly observed in D factor of that bond (Fig. 9.12). The seemingly isolated H6 atom strengthens its bond to C2 (Fig. 9.11(A)), its interactions with other protons in the system are hardly noticeable on its fragility diagrams.

9.7.4 Summary of the indicators for monitoring reactions

Our theoretical and computational analysis of the chemical reaction delivers understanding of its fine details. Here we have presented a systematic review of the utility of the novel tools, accessible with the computational quantum chemistry methods. With the use of the cumulative force constants C_{AB}, the method allows assessing the bond stability, rather than the bond energy, in some sort of analogy to the standard normal mode analysis. There are two important advantages in our reaction fragility approach over the normal modes evolution along the reaction path: (i) reaction fragilities are given by the electron energy exclusively and (ii) they are focused directly on atoms and bonds, the indispensable objects for chemical considerations.

The eigenvalues and eigenvectors for the lowest atomic fragility modes for a system provide the first indication on the location of the reaction center, and also allow for detection the outreach of the process to atoms affected, though distant from a reaction center. Further global insight is provided by the global electron energy derivatives K_ξ and A_ξ. It is interesting to note that in the atomic units, the numerical values of the elements of the DF connectivity matrix and their derivatives cover the orders of magnitude convenient for the facile comparison between various systems and reactions. The nature of K_ξ and A_ξ indicators is, however, different from the two basic global indicators: the trace of the connectivity matrix and its derivative known as the reaction fragility, $Tr\underline{\underline{\mathbf{C}}}$ and $a_\xi = d(Tr\underline{\underline{\mathbf{C}}})/d\xi$, respectively. These two allow for observation of a system in an electron stationary state, whereas the K_ξ and A_ξ contain an additional information on the reaction path: the D_{AB} factor that includes the distance changes on a step. Hence, K_ξ and A_ξ characterize a nature of the particular step on IRC, rather that the system itself.

The atomic and bond fragilities are two types of indicators for observation the individual atoms, the natural components of any reacting system. As demonstrated on the example (Section 9.6.5), they describe convincingly the degree of

coupling of an atom in a particular position in a molecule, not only by a bond to particular neighboring atom, but through the electronic interactions, to the complete network of atoms in the entire system. Together with the squares of the normalized atomic coefficients of the eigenvectors, they provide most valuable information on the role of every atom in the transition process from reactants to products.

The tools for observation of bonds in a reacting system are complementary to those developed for atoms. The bond fragilities $a_{\xi}^{AB} = -dC_{AB}/d\xi$ describe the variations in the bond orders, as the elements C_{AB} have the familiar meaning of the cumulative force constant for particular bonds, with their meaning limited to the electron energy. As demonstrated in Section 9.6.5 and discussed in Section 9.7.3 for the internal proton transfer in formamide, the bond fragilities are sensitive indicators of the interactions even as weak as between the two hydrogen atoms separated by a chain of 2–3 other atoms. This appears to be more attractive for the chemical discussion of the electron density modification in a reaction than the calculation of the actual force constants for the virtual oscillators (the normal modes).

The energy analysis presented in this work provides a new tool for observation bonds as they are created or modified in reactions. The D_{AB} parameters calculated for bonds might serve as detectors of the actual limits for a process on a reaction path – the points of its onset and decay. They also clearly point out to the moving atoms in a system discerning them from the ones that are merely adapting.

The bond components to the K_{ξ} value provide possibly the most perspicuous view of the changes in a reacting system, by discerning the energy inputs required not only for a bond creation or rupture, but also for tiny modifications of any contact between atoms in a system. The sequence of the oncoming reaction events is also clearly illustrated by these bond components. The components of the associated third derivative of the energy (A_{ξ}) are considerable less sensitive probes for a reaction. They do, however, discern between the bond breaking and bond formation process, therefore, they may play an essential subsidiary role in describing a reaction mechanism.

9.8 Conclusions and perspectives

The methodology presented in this work has been built on the computational results available in the Cartesian Hessian, the concept is parallel to that presented by Seminario in his FUERZA method [83]. This author demonstrated how to derive the internal force constants for chosen bonds and angles (with sufficient accuracy), by the procedure beyond the normal mode analysis. The goal of this present work is similar, however it is considerably broader, more intricate, and reaching deeply into the nature of the interactions between atoms. The Cartesian Hessian has once again been explored as a reliable source of data with facile computational access. By exploring the vector analysis (divergence

of force, rather than the ordinary derivatives), the Cartesian Hessian ($3n \times 3n$) is contracted to the Density Functional connectivity matrix ($n \times n$) whose elements not only describe all mutual interactions between atoms nested inside their molecular environment, but also report the electronic energy exclusively.

This effect has been first noted by W. T. King in his early works [47–49]. The author had described the frequency sum rule and understood the electronic energy behind it [47]: *"the effective Cartesian force constants found by this sum rule are independent of the nuclear repulsion energy and consequently depend only on the electron distribution in the molecule."* An additional conclusion deals with the Born–Oppenheimer approximation inherent in his work. "*Because the nuclear-repulsion energy*, (. . .) *is an additive term in the potential function and because it satisfies Laplace's equation, it will vanish in the calculation of* $[\nabla^2 E]$ *by any method*. (. . .)" [48]. The far reaching consequences of King's findings have not been explored until in this present work. The existing apparatus of the Conceptual DFT and the contemporary computational tools allowed for the development both of the theory and applications of this effect oriented for practical chemistry.

By defining the DF connectivity matrix and by formulation of the H–F force divergences in the language of the Conceptual DFT, an extension has been accomplished for the King's formula presented in the language of physics. A connection between the matrix elements of purely electronic nature and the linear response function has been demonstrated [46]. The break-through in the theory has been achieved by exploring the general property of the density function, theoretically proved by S. Liu et al. [80] (cf. Appendix 9.A.2). Its application to the DF Connectivity Matrix resulted in the uniform formulation of the matrix elements (Scheme 9.1). The original gradient theorem equally applicable for open and closed systems (Eqs. (9.6) and (9.12)) has been developed on this ground. With the above findings, the vibrational energy term in the energy expansion has been proved to be purely electronic in its nature.

There are important consequences of the above result, to name a few. The vibrational energy can now be expressed as a sum of contributions from bonds and contacts between atoms, much in the spirit of chemical discussions of their properties. That resolves the problem raised by Seminario [83], and recently discussed by S. Racioppi et al. [101] referring the methods for the breakdown of interaction energy, an important tool to understand chemical bonding. By proving the DFT formulae for the elements of the DF Connectivity Matrix C_{AA}, C_{AB} (Scheme 9.1) an *a priori* quantitative method for description of atoms and bonds has been achieved. This finding tends to undermine the assertion once expressed by Parr and Nalewajski: "*the atom in a molecule cannot be directly observed by experiment, nor can one measure enough properties of an atom in a molecule to define it unambiguously*" [14]. Properties of an atom may, nonetheless, be quantified by present reaction fragility method focused on interactions of the actual density function with an atomic nuclei. (A similar point of view has been a source of the nuclear magnetic resonance method.) We present the energy

analysis that leads to diagonalization of the energy matrix in atomic resolution; this is formally parallel to the Charge Sensitivity Analysis (CSA) by Nalewajski et al. [43,44,102]. However, unlike the CSA method where atomic populations have been assigned to atoms with a selected arbitrary definition, the electronic energy function in our approach rests entirely on the physical and computable quantities, namely electric field vector and H–F forces.

The observation method for variable bond orders and atomic valences on a reaction path is the valuable practical application of the DF Connectivity Matrix [52,63,72]. We have proved that the derivatives of the DF connectivity matrix elements with respect to the reaction progress parameters (Reaction Fragilities) serve as fine probes of the electron density evolution upon a reaction. This observation is focused directly on the valence region of a reacting molecule, as it has been noticed by Salem, that core electron region of the spherical symmetry does not contribute to the electronic H–F force acting on a nucleus [51]. The energy analysis presented hereby provided the justification for the Reaction Fragility Method: the bond fragilities represent a measure for the anharmonicity of bonds and contacts in the actual configuration of the nuclei at the corresponding stationary state of the electron density. In the chemical language, anharmonicity can be translated as the susceptibility of a bond to changing its strength, the formidable point of view for a chemist interested in transformations of molecules – chemical reactions.

The theoretical results may also facilitate the deeper understanding of the mechanism of the molecular transformation. The first and dominating term in the energy expansion (Eqs. (9.25) and (9.28)) is the reaction force work; the energy required to shift the nuclei to new positions on a reaction step. In an actual reaction, this energy is likely to be provided by a collision, resulting in a nonequilibrium excited state (vibrational or electronic) and possibly the starting point for further process leading to a new state of equilibrium. In order to apply the reaction fragility analysis to monitoring the electronic structure of such system on its way, the coupling with the direct dynamics simulation might be considered [103]. Combining with the reaction fragility method would open the direct dynamics simulations to exploration by chemists and could allow widening the studies on reactions beyond the IRC regime.

Acknowledgments

The authors are pleased to acknowledge their cooperation with Mr Mateusz Jędrzejewski and Mr Jarosław Zaklika, who provided the numerical data, necessary for illustration of this article. The discussion of the example in this present work has been based on the computational data published as the joint work of the group (references [77] and [95]); the use of resources of Wrocław Center for Networking and Supercomputing in these projects is gratefully acknowledged (WCSS Grants No. 249 and GW 036). PO acknowledges the support by the university grant POMOST N110/0004/21. The enlightening discussions with Dr Jerzy Hładyszowski were much helpful. This paper has been submitted to the editor on March 31st, 2021, and in final form on October 31st, 2021.

Appendix 9.A Auxiliary notation and proofs for the relations appearing in the text

9.A.1 Notation

The following notation for electron density gradients and the electric fields has been adopted throughout the paper:

$$\nabla\rho(\mathbf{r}) = \frac{\partial\rho(\mathbf{r})}{\partial\mathbf{r}}, \tag{9.A.1}$$

$$\nabla_A v(\mathbf{r}) = \frac{\partial v(\mathbf{r})}{\partial\mathbf{R}_A} = -\boldsymbol{\varepsilon}_A(\mathbf{r}) \quad \text{and} \quad \Delta v(\mathbf{r}) = -\sum_A \boldsymbol{\varepsilon}_A(\mathbf{r})\cdot\Delta\mathbf{R}_A. \tag{9.A.2}$$

If not marked otherwise, the following equivalent notation for the density gradient is used:

$$\boldsymbol{\nabla}_A\rho(\mathbf{r}) = \left[\frac{\partial\rho(\mathbf{r})}{\partial\mathbf{R}_A}\right]_N = [\boldsymbol{\nabla}_A\rho(\mathbf{r})]_N\,. \tag{9.A.3}$$

9.A.2 Proof of Eq. (9.1)

Explicit relations between the divergences of H–F force (Eqs. (9.1) and (9.3)) and the electron density function have been demonstrated in the previous paper from this laboratory [46] as

$$C_{AA} = (\boldsymbol{\nabla}_A\cdot\mathbf{F}_A)_N = 4\pi Z_A\rho(\mathbf{R}_A) + \int \boldsymbol{\varepsilon}_A(\mathbf{r})\cdot[\boldsymbol{\nabla}_A\rho(\mathbf{r})]_N\,d\mathbf{r}, \tag{9.A.4}$$

$$C_{B\neq A} = (\boldsymbol{\nabla}_A\cdot\mathbf{F}_A)_N = \int \boldsymbol{\varepsilon}_A(\mathbf{r})\cdot\left[\boldsymbol{\nabla}_{B\neq A}\rho(\mathbf{r})\right]_N d\mathbf{r}. \tag{9.A.5}$$

An equation equivalent to (9.A.4) was first reported by King [48]. The role of density at the nucleus in Eq. (9.A.4) has been unclear since $\rho(\mathbf{R}_A)\neq 0$ [104, 105]. It may be eliminated, by exploring the general result elaborated by Shubin Liu et al. [80],

$$\rho(\mathbf{R}_A) = -\frac{1}{4\pi}\int\frac{(\mathbf{r}-\mathbf{R}_A)\cdot\nabla\rho(\mathbf{r})}{|\mathbf{r}-\mathbf{R}_A|^3}d\mathbf{r}. \tag{9.A.6}$$

By using this result, Eq. (9.A.4) is transformed to a novel form containing the electron density function $\rho(\mathbf{r})$ as the only variable parameter; it is now analogous to the expression for the nondiagonal elements of the DF connectivity matrix (Eq. (9.1), main text),

$$C_{AA} = \int \boldsymbol{\varepsilon}_A(\mathbf{r})\cdot[\nabla\rho(\mathbf{r}) + \boldsymbol{\nabla}_A\rho(\mathbf{r})]\,d\mathbf{r}. \tag{9.A.7}$$

Since for a single atom $\nabla\rho(\mathbf{r}) = -\nabla_A\rho(\mathbf{r})$, Eq. (9.A.7) properly explains why $C_{AA} = 0$ for a noninteracting atom, otherwise $C_{AA} > 0$, as has been demonstrated.

Another valuable conclusion arises when properties of the density gradient are recalled. The integral in Eq. (9.A.7) calculated for an atom can be finite if and only if $\lim_{\mathbf{r}\to 0}[\nabla\rho(\mathbf{r}) + \nabla_A\rho(\mathbf{r})] = 0$ since $\boldsymbol{\varepsilon}_A(\mathbf{r}) \to \infty$ for $\mathbf{r} \to 0$. Since the cusp condition requires $\nabla\rho(0)$ to be finite, an additional general condition emerges for the electron density at a nucleus, namely $\lim_{\mathbf{r}\to 0}\nabla\rho(\mathbf{r}) = -\lim_{\mathbf{r}\to 0}\nabla_A\rho(\mathbf{r})$. This condition appears to be independent on the state of bonding of atom, as is the cusp condition itself.

9.A.3 The dyadic product of vectors (Eq. (9.15))

$$[\nabla_B \otimes \mathbf{F}_A] \equiv \begin{bmatrix} \partial F_{Ax}/\partial R_{Bx} & \partial F_{Ay}/\partial R_{Bx} & \partial F_{Az}/\partial R_{Bx} \\ \partial F_{Ax}/\partial R_{By} & \partial F_{Ay}/\partial R_{By} & \partial F_{Az}/\partial R_{By} \\ \partial F_{Ax}/\partial R_{Bz} & \partial F_{Ay}/\partial R_{Bz} & \partial F_{Az}/\partial R_{Bz} \end{bmatrix}. \tag{9.A.8}$$

9.A.4 Proof of Eq. (9.26)

The essential property of the DF connectivity matrix is used first, $\sum_A C_{AB} = 0$. Then

$$\begin{aligned} \sum_A \sum_B (\Delta\mathbf{R}_A \cdot \Delta\mathbf{R}_B)\, C_{AB} &= \\ &= \sum_A \sum_{B\neq A} (\Delta\mathbf{R}_A \cdot \Delta\mathbf{R}_B)\, C_{AB} + \sum_A (\Delta\mathbf{R}_A)^2\, C_{AA} = \\ &= \sum_A \sum_{B\neq A} (\Delta\mathbf{R}_A \cdot \Delta\mathbf{R}_B)\, C_{AB} - \sum_A (\Delta\mathbf{R}_A)^2 \sum_{B\neq A} C_{AB}. \end{aligned} \tag{9.A.9}$$

Since $C_{AB} = C_{BA}$, the first term in this result becomes

$$\sum_A \sum_{B\neq A} (\Delta\mathbf{R}_A \cdot \Delta\mathbf{R}_B)\, C_{AB} = 2\sum_A \sum_{B<A} (\Delta\mathbf{R}_A \cdot \Delta\mathbf{R}_B)\, C_{AB}. \tag{9.A.10}$$

The second term of the result (Eq. (9.A.9)) may be divided into two equal parts:

$$\sum_A (\Delta\mathbf{R}_A)^2 \sum_{B\neq A} C_{AB} = \sum_A (\Delta\mathbf{R}_A)^2 \sum_{B<A} C_{AB} + \sum_B (\Delta\mathbf{R}_B)^2 \sum_{A<B} C_{BA}. \tag{9.A.11}$$

Summations over A and B in Eq. (9.A.11) are equivalent, hence by substituting Eqs. (9.A.10) and (9.A.11) into Eq. (9.A.9), and selecting the pairs AB, leads to

the final result:

$$
\begin{aligned}
&2\sum_{A}\sum_{B<A}(\Delta\mathbf{R}_A\cdot\Delta\mathbf{R}_B)\,C_{AB}-\\
&\quad-\left[\sum_{A}(\Delta\mathbf{R}_A)^2\sum_{B<A}C_{AB}+\sum_{B}(\Delta\mathbf{R}_B)^2\sum_{A<B}C_{BA}\right]=\\
&=-\sum_{A}\sum_{B<A}C_{AB}\left[(\Delta\mathbf{R}_A)^2-2\Delta\mathbf{R}_A\cdot\Delta\mathbf{R}_B+(\Delta\mathbf{R}_B)^2\right]=\\
&=-\sum_{A}\sum_{B<A}C_{AB}\,(\Delta\mathbf{R}_A-\Delta\mathbf{R}_B)^2=-\sum_{A}\sum_{B<A}C_{AB}\,|\Delta(\mathbf{R}_A-\mathbf{R}_B)|^2\\
&=-\sum_{A}\sum_{B<A}C_{AB}\,|\Delta\mathbf{R}_{AB}|^2
\end{aligned}
\tag{9.A.12}
$$

References

[1] R.G. Parr, W. Yang, Density Functional Theory of Atoms and Molecules, Oxford University Press, Oxford, UK, 1989.

[2] H. Chermette, Chemical reactivity indexes in density functional theory, J. Comput. Chem. 20 (1999) 129–154.

[3] P. Geerlings, F. De Proft, W. Langenaeker, Conceptual density functional theory, Chem. Rev. 103 (2003) 1793–1874.

[4] P. Geerlings, E. Chamorro, P.K. Chattaraj, F. De Proft, J.L. Gázques, S. Liu, C. Morell, A. Toro-Labbé, A. Vela, P.W. Ayers, Conceptual density functional theory: status, prospects, issues, Theor. Chem. Acc. 139 (2020) 36.

[5] P.W. Ayers, R.C. Morrison, R.K. Roy, Variational principles for describing chemical reactions: condensed reactivity indices, J. Chem. Phys. 116 (2002) 8731–8744.

[6] R.F. Nalewajski, J. Korchowiec, Z. Zhou, Molecular hardness and softness parameters and their use in chemistry, Int. J. Quantum Chem., Symp. 22 (1988) 349–366.

[7] N. Sablon, F. De Proft, P.W. Ayers, P. Geerlings, Computing Fukui functions without differentiating with respect to electron number. II. Calculation of condensed molecular Fukui functions, J. Chem. Phys. 126 (2007) 224108.

[8] P. Fuentealba, P. Pérez, R. Contreras, On the condensed Fukui function, J. Chem. Phys. 113 (2000) 2544–2551.

[9] P. Bultinck, S. Fias, C. Van Alsenoy, P.W. Ayers, R. Carbó-Dorca, Critical thoughts on computing atom condensed Fukui functions, J. Chem. Phys. 127 (2007) 034102.

[10] L. Komorowski, J. Lipiński, P. Szarek, Polarization justified Fukui functions, J. Chem. Phys. 131 (2009) 124120.

[11] L. Komorowski, J. Lipiński, P. Szarek, P. Ordon, Polarization justified Fukui functions: theory and applications for molecules, J. Chem. Phys. 135 (2011) 014109.

[12] C. Cardenas, E. Echegaray, D. Chakraborty, J.S.M. Anderson, P.W. Ayers, Relationships between the third-order reactivity indicators in chemical density-functional theory, J. Chem. Phys. 130 (2009) 244105.

[13] R.F.W. Bader, Atoms in Molecules. A Quantum Theory, International Series of Monographs in Chemistry, vol. 22, A Clarendon Press Publication, 1994.

[14] R.G. Parr, P.W. Ayers, R.F. Nalewajski, What is an atom in a molecule?, J. Phys. Chem. A 109 (2005) 3957–3959.

[15] P. Geerlings, S. Fijas, Z. Boisdenghien, F. De Proft, Conceptual DFT: chemistry from the linear response function, Chem. Soc. Rev. 43 (2014) 4989–5008.

[16] Z. Boisdenghien, C. Van Alsenoy, F. De Proft, P. Geerlings, Evaluating and interpreting the chemical relevance of the linear response kernel for atoms, J. Chem. Theory Comput. 9 (2013) 1007–1015.
[17] Z. Boisdenghien, S. Fias, C. Van Alsenoy, F. De Proft, P. Geerlings, Evaluating and interpreting the chemical relevance of the linear response kernel for atoms II: open shell, Phys. Chem. Chem. Phys. 16 (2014) 14614–14624.
[18] Z. Boisdenghien, S. Fias, F. Da Pieve, F. De Proft, P. Geerlings, The polarizability of atoms and molecules: a comparison between a conceptual density functional theory approach and time-dependent density functional theory, Mol. Phys. 113 (13–14) (2015) 1890–1898.
[19] A. Vela, J.L. Gazquez, A relationship between the static dipole polarizability, the global softness, and the Fukui function, J. Am. Chem. Soc. 112 (1990) 1490–1492.
[20] J. Garza, J. Robles, Density-functional-theory softness kernel, Phys. Rev. 47 (1993) 2680–2685.
[21] Y. Li, N.S. Evans, The Fukui function: a key concept linking frontier molecular orbital theory and the hard-soft-acid-base principle, J. Am. Chem. Soc. 117 (1995) 7756–7759.
[22] W. Beker, A. Stachowicz-Kuśnierz, J. Zaklika, A. Ziobro, P. Ordon, L. Komorowski, Atomic polarization justified Fukui indices and the affinity indicators in aromatic heterocycles and nucleobases, Comput. Theor. Chem. 1065 (2015) 42–49.
[23] N. Sablon, F. De Proft, P. Geerlings, The linear response kernel: inductive and resonance effects quantified, J. Phys. Chem. Lett. 1 (2010) 1228–1234.
[24] B.G. Baekelandt, The nuclear Fukui function and Berlin's binding function in density functional theory, J. Chem. Phys. 105 (1996) 4664–4667.
[25] P. Ordon, L. Komorowski, Nuclear reactivity and nuclear stiffness in density functional theory, Chem. Phys. Lett. 292 (1998) 22–27.
[26] F. De Proft, S. Liu, P. Geerlings, Calculation of the nuclear Fukui function and new relations for nuclear softness and hardness kernels, J. Chem. Phys. 108 (1998) 7549–7554.
[27] R. Balawender, P. Geerlings, Nuclear Fukui function from coupled perturbed Hartree–Fock equations, J. Chem. Phys. 114 (2001) 682–691.
[28] R.P. Feynman, Forces in molecules, Phys. Rev. 56 (1939) 340–343.
[29] M. Novák, J. Vackáře, R. Cimrman, Evaluating Hellmann–Feynman forces within non-local pseudopotentials, Comput. Phys. Commun. 250 (2020) 107034e.
[30] H. Nakatsuji, Electron-cloud following and preceding and the shapes of molecules, J. Am. Chem. Soc. 96 (1974) 30–37.
[31] H. Nakatsuji, Electrostatic force theory for a molecule and interacting molecules. I. Concept and illustrative applications, J. Am. Chem. Soc. 95 (1973) 345–353.
[32] M.H. Cohen, M.V. Ganduglia-Pirovano, J. Kudrnovsky, Electronic and nuclear chemical reactivity, J. Chem. Phys. 101 (1994) 8988–8997.
[33] B.G. Baekelandt, A. Cedillo, R.G. Parr, Reactivity indexes and fluctuation formulas in density functional theory: isomorphic ensembles and a new measure of local hardness, J. Chem. Phys. 103 (1995) 8548–8556.
[34] M. Berkowitz, S.K. Ghosh, R.G. Parr, On the concept of local hardness in chemistry, J. Am. Chem. Soc. 107 (1985) 6811–6814.
[35] R. Laplaza, C. Cárdenas, P. Chaquin, J. Contreras-García, P.W. Ayers, Orbital energies and nuclear forces in DFT: interpretation and validation, J. Comput. Chem. 42 (5) (2021) 334–343.
[36] P. Ordon, L. Komorowski, DFT energy derivatives and their renormalization in molecular vibrations, Int. J. Quant. Chem. 101 (2005) 703–713.
[37] L. Komorowski, P. Ordon, Anharmonicity of a molecular oscillator, Int. J. Quant. Chem. 99 (2004) 153–160.
[38] L. Komorowski, P. Ordon, Vibrational softening of diatomic molecules, Theor. Chem. Acc. 105 (2001) 338–344.
[39] L. Komorowski, P. Ordon, Fluctuations in electronegativity and global hardness induced by molecular vibrations, J. Mol. Struct., Theochem 630 (2003) 25–32.

[40] L. Komorowski, P. Ordon, DFT analysis of fluctuations in electronegativity and hardness of a molecular oscillator, Int. J. Quant. Chem. 91 (2003) 398–403.
[41] T. Luty, P. Ordon, C.J. Eckhardt, A model for mechanochemical transformations: applications to molecular hardness, instabilities, and shock initiation of reaction, J. Chem. Phys. 117 (2002) 1775–1785.
[42] P. Ordon, PhD Thesis, Wrocław University of Technology, 2003.
[43] R.F. Nalewajski, J. Korchowiec, Charge Sensitivity Approach to Electronic Structure and Chemical Reactivity, World-Scientific, Singapore, 1997, and references therein.
[44] B.G. Baekelandt, G.O.A. Janssens, H. Toufar, W.J. Mortier, R.A. Schoonheydt, R.F. Nalewajski, Mapping between electron population and vibrational normal modes within the charge sensitivity analysis, J. Phys. Chem. 99 (1995) 9784–9794.
[45] R.F. Nalewajski, A coupling between the equilibrium state variables of open molecular and reactive systems, Phys. Chem. Chem. Phys. 1 (1999) 1037–1049.
[46] P. Ordon, L. Komorowski, M. Jędrzejewski, Conceptual DFT analysis of the fragility spectra of atoms along the minimum energy reaction coordinate, J. Chem. Phys. 147 (2017) 134109.
[47] W.T. King, A.J. Zelano, Sum rule for molecular frequencies, J. Chem. Phys. 46 (1967) 3197–3199.
[48] W.T. King, Calculation of molecular force constants, J. Chem. Phys. 49 (1968) 2866–2867.
[49] W.T. King, Calculation of atomic force constants from electron densities, J. Chem. Phys. 57 (1972) 4535–4539.
[50] J.C. Decius, E.B. Wilson, Sum rules for the vibration frequencies of isotopic molecules, J. Chem. Phys. 19 (1951) 1409–1412.
[51] L. Salem, Theoretical interpretation of force constants, J. Chem. Phys. 38 (1963) 1227–1236.
[52] L. Komorowski, P. Ordon, M. Jędrzejewski, The reaction fragility spectrum, Phys. Chem. Chem. Phys. 18 (2016) 32658–32663.
[53] L. Spialter, The atom connectivity matrix (ACM) and its characteristic polynomial (ACMCP): a new computer-oriented chemical nomenclature, J. Am. Chem. Soc. 85 (1963) 2012–2013.
[54] L. Spialter, The atom connectivity matrix (ACM) and its characteristic polynomial (ACMCP), J. Chem. Doc. 4 (1964) 261–269.
[55] E. Hyde, F.W. Matthews, L.H. Thomson, W.J. Wiswesser, Conversion of Wiswesser notation to a connectivity matrix for organic compounds, J. Chem. Doc. 7 (1967) 200–204.
[56] Y. Kudo, T. Yamasaki, S. Sasaki, The characteristic polynomial uniquely represents the topology of a molecule, J. Chem. Doc. 13 (1973) 225–227.
[57] M.F. Thorpe, F.L. Galeener, Network dynamics, Phys. Rev. B 22 (1980) 3078–3092.
[58] S.C. Basak, V.R. Magnuson, G.J. Niemi, R.R. Regal, Determining structural similarity of chemicals using graph-theoretical indices, Discrete Appl. Math. 19 (1988) 17–44.
[59] M. Sato, Hamiltonian graph representation of zeolite frameworks and Si, Al ordering in the framework, J. Math. Chem. 7 (1991) 341–352.
[60] A.L. Mackay, Generalized structural geometry, Acta Crystallogr. A30 (1974) 440–447.
[61] M. O'Keeffe, A method for calculating bond valences in crystals, Acta Crystallogr. A46 (1990) 138–142.
[62] I. Mayer, Bond orders and valence indices, J. Comput. Chem. 28 (2007) 204–211.
[63] J. Zaklika, L. Komorowski, P. Ordon, The bond fragility spectra for the double proton transfer reaction, in the formic acid type dimers, J. Phys. Chem. A 123 (2019) 4274–4283.
[64] D. Cremer, A. Wu, E. Kraka, The mechanism of the reaction $FH+H_2C{=}CH_2 \rightarrow H_3C{-}CFH_2$. Investigation of hidden intermediates with the unified reaction valley approach, Phys. Chem. Chem. Phys. 3 (2001) 674–687.
[65] Z. Konkoli, E. Kraka, D. Cremer, Unified reaction valley approach mechanism of the reaction $CH_3 + H_2 \rightarrow CH_4 + H$, J. Phys. Chem. A 101 (1997) 1742–1757.
[66] E. Kraka, W. Zou, Y. Tao, M. Freindorf, Exploring the mechanism of catalysis with the unified reaction valley approach (URVA) – a review, Catalyst 10 (2020) 691.

[67] Z. Konkoli, D.A. Cremer, New way of analyzing vibrational spectra. I. Derivation of adiabatic internal modes, Int. J. Quant. Chem. 67 (1998) 1–9.
[68] Z. Konkoli, A. Larsson, D. Cremer, A new way of analyzing vibrational spectra. II. Comparison of internal mode frequencies, Int. J. Quant. Chem. 67 (1998) 11–27.
[69] Z. Konkoli, D. Cremer, A new way of analyzing vibrational spectra. III. Characterization of normal vibrational modes in terms of internal vibrational modes, Int. J. Quant. Chem. 67 (1998) 29–40.
[70] Z. Konkoli, A. Larsson, D. Cremer, A new way of analyzing vibrational spectra. IV. Application and testing of adiabatic modes within the concept of the characterization of normal modes, Int. J. Quant. Chem. 67 (1998) 41–55.
[71] E. Kraka, W. Zou, Y. Tao, Decoding chemical information from vibrational spectroscopy data: local vibrational mode theory, WIREs Comput. Mol. Sci. 10 (2020) e1480.
[72] J. Zaklika, L. Komorowski, P. Ordon, Evolution of the atomic valence observed by the reaction fragility spectra on the reaction path, J. Mol. Model. 25 (2019) 134.
[73] A. Toro-Labbé, S. Gutiérrez-Oliva, J.S. Murray, P. Politzer, A new perspective on chemical and physical processes: the reaction force, Mol. Phys. 105 (2007) 2619–2625.
[74] L. Piela, Ideas of Quantum Chemistry, Elsevier, Amsterdam N.L., 2007.
[75] M. Jędrzejewski, P. Ordon, L. Komorowski, Atomic resolution for the energy derivatives on the reaction path, J. Phys. Chem. A 120 (2016) 3780–3787.
[76] W.H. Miller, N.C. Handy, J.E. Adams, Reaction path Hamiltonian for polyatomic molecules, J. Chem. Phys. 72 (1980) 99–112.
[77] P. Ordon, L. Komorowski, M. Jędrzejewski, J. Zaklika, The connectivity matrix: a toolbox for monitoring bonded atoms and bonds, J. Phys. Chem. A 124 (6) (2020) 1076–1086.
[78] R. Inostroza-Rivera, M. Yahia-Ouhmed, V. Tognetti, L. Joubert, B. Herrera, A. Toro-Labbé, Atomic decomposition of conceptual DFT descriptors: application to proton transfer reactions, Phys. Chem. Chem. Phys. 17 (2015) 17797–17807.
[79] E. Vöhringer-Martinez, A. Toro-Labbé, Understanding the physics and chemistry of reaction mechanisms from atomic contributions: a reaction force perspective, J. Phys. Chem. A 116 (2012) 7419–7423.
[80] S. Liu, R.G. Parr, A. Nagy, Cusp relations for local strongly decaying properties in electronic systems, Phys. Rev. A 52 (1995) 2645–2651.
[81] P. Hohenberg, W. Kohn, Inhomogeneous electron gas, Phys. Rev. 136 (1964) 8864–8871.
[82] M. Berkowitz, R.G. Parr, Molecular hardness and softness, local hardness and softness, hardness and softness kernels, and relations among these quantities, J. Chem. Phys. 88 (1988) 2554–2557.
[83] J.M. Seminario, Calculation of intramolecular force fields from second-derivative tensors, Int. J. Quantum Chem., Symp. 30 (1996) 1271–1277.
[84] https://en.wikipedia.org/wiki/Dyadics#Dyadic_algebra. (Accessed 19 January 2021).
[85] J.W. Gibbs, Vector Analysis, Dover Publishing, New York, 1960, p. 306.
[86] E.B. Wilson Jr., J.C. Decius, P.C. Cross, Molecular Vibrations, Dover Publications, New York, USA, 1980.
[87] S.J. Cyvin, Molecular Vibrations and Mean Square Amplitudes, Elsevier, Amsterdam, NL, 1968.
[88] P. Ordon, A. Tachibana, Use of nuclear stiffness in search for a maximum hardness principle and for the softest states along the chemical reaction path: a new formula for the energy third derivative γ, J. Chem. Phys. 126 (2007) 234115.
[89] D. Yepes, J.S. Murray, P. Politzer, P. Jaque, The reaction force constant: an indicator of the synchronicity in double proton transfer reactions, Phys. Chem. Chem. Phys. 14 (2012) 11125–11134.
[90] D. Yepes, O. Donoso-Tauda, P. Perez, J.S. Murray, P. Politzer, P. Jaque, The reaction force constant as an indicator of synchronicity/nonsynchronicity in [4+2] cycloaddition processes, Phys. Chem. Chem. Phys. 15 (2013) 7311–7320.

[91] A. Toro-Labbé, Characterization of chemical reactions from the profile of energy, chemical potential, and hardness, J. Phys. Chem. A 103 (1999) 4398–4403.
[92] E. Kraka, D. Cremer, Computational analysis of the mechanism of chemical reactions in terms of reaction phases: hidden intermediates and hidden transition states, Acc. Chem. Res. 43 (2010) 591–601.
[93] W. Zou, T. Sexton, E. Kraka, M. Freindorf, D. Cremer, A new method for describing the mechanism of a chemical reaction based on the unified reaction valley approach, J. Chem. Theory Comput. 12 (2016) 650–663.
[94] M. Frisch, G. Trucks, H. Schlegel, G. Scuseria, M. Robb, J. Cheeseman, G. Scalmani, V. Barone, B. Mennucci, G. Petersson, GAUSSIAN 09 (Revision A.02), Inc., Wallingford, CT, 2009.
[95] P. Ordon, J. Zaklika, M. Jędrzejewski, L. Komorowski, Bond softening indices studied by the fragility spectra for proton migration in formamide and related structures, J. Phys. Chem. A 124 (2020) 328–338.
[96] J.W. Ochterski, Vibrational analysis in Gaussian, https://gaussian.com/vib/. (Accessed 19 January 2021).
[97] https://github.com/numpy/numpy/tree/v1.17.2. (Accessed 28 October 2019).
[98] T.E. Oliphant, A Guide to NumPy, Trelgol Publishing, USA, 2006.
[99] S. Van der Walt, C.S. Colbert, G. Varoquaux, The NumPy array: a structure for efficient numerical computation, Comput. Sci. Eng. 13 (2011) 22–30.
[100] https://matrixcalc.org/pl/. (Accessed 30 November 2020).
[101] S. Racioppi, A. Sironi, P. Macchi, On generalized partition method for interaction energies, Phys. Chem. Chem. Phys. 22 (2020) 24291–24298.
[102] R.F. Nalewajski, The hardness based molecular charge sensitivities and their use in the theory of chemical reactivity, in: K.D. Sen (Ed.), Chemical Hardness, Struct. Bond. 80 (1993) 115–186.
[103] S. Pratihar, Xi. Ma, Z. Homayoon, G.L. Barnes, W.L. Hase, Direct chemical dynamics simulations, J. Am. Chem. Soc. 139 (2017) 3570–3590.
[104] T. Kato, On the eigenfunctions of many-particle systems in quantum mechanics, Commun. Pure Appl. Math. 10 (1957) 151–177.
[105] P.K. Chattaraj, A. Cedillo, R.G. Parr, Fukui function for a gradient expansion formula, and estimate of hardness and covalent radius for an atom, J. Chem. Phys. 103 (1995) 10621–10626.